

Erosion Stability of Wide-Graded Quarry-Stone Material under Unidirectional Current

A. Schendel¹; N. Goseberg²; and T. Schlurmann³

Abstract: Scour protection around hydraulic structures in fluvial, estuarine, and coastal waters is an essential component of a meaningful and durable design. The continuous optimization of scour protection systems and design approaches leads to faster and more cost-effective construction processes. Although scour protection now often consists of a two-layer design, approaches that incorporate only one layer depict a major step forward. Therefore, this research focuses on the stability of a wide-graded quarry-stone mixture consisting of crushed granodiorite (Jelsa quarry, Norway) with fractions ranging from 0.063 to 200 mm. The material was exposed to an incrementally increased unidirectional current in a closed-circuit flume. The induced flow field and leading parameters were measured at various positions horizontally and vertically, whereas the erosion rates were determined behind the test bed specimen. With increasing flow velocity the development of a static armor layer was observed at the bed surface. Bed-shear stresses were determined to be strongly variable across the rough test bed. Fractional critical shear stresses indicate highly selective mobility of individual fractions. Least-square fitting of the determined critical shear stresses based on the dimensionless reference grain size d_i/d_σ (with d_σ as the product of the geometric mean size d_g and the geometric standard deviation σ_g) is suitable for describing the stability behavior of the investigated material. DOI: [10.1061/\(ASCE\)WW.1943-5460.0000321](https://doi.org/10.1061/(ASCE)WW.1943-5460.0000321). This work is made available under the terms of the Creative Commons Attribution 4.0 International license, <http://creativecommons.org/licenses/by/4.0/>.

Author keywords: Scour protection; Laboratory tests; Erosion stability; Shear stress; Incipient motion.

Introduction

Wide-graded quarry-stone mixtures depict a suitable material for the majority of bed protection constructions and toe and slope stabilizations in hydraulic and ocean engineering, although its potential as an innovative bed or scour protection system has not been fully revealed. Due to their versatility, flexibility, and cost-efficient production, wide-graded materials seem economically and hydraulically feasible compared with other bed and slope protection systems. One reason for this is that wide-graded materials can be applied as discrete single-layer bed or scour protection without an additional filter layer by adjusting the grain size distribution to geotechnical and hydraulic filter requirements. Although recent studies have examined the stability of a scour protection that contains a single stone cover above an additional filter layer (Sumer and Nielsen 2013; Nielsen et al. 2013; De Schoesitter et al. 2014), to the authors' knowledge, so far no research has been performed in the investigation of a scour protection design that integrates the functions of the filter and cover layer in one single layer. Wolters and van Gent (2012) and Schürenkamp et al. (2014) performed experiments on

the stability of geometrically open filters, which are characterized by a large ratio of the size of top-layer material and sublayer material. While these studies focused on the interface stability between base and filter layer and on the transport of base material, the erosion stability of a single-layer filter against external hydrodynamic loading was not considered.

Another benefit of wide-graded materials is the ease of placement by excavators and slides or by other means. As scour protection, the verification of the erosion stability, performance, and durability of wide-graded material mixtures to external influences such as currents or waves is of major importance. To design a stable mineral scour protection it is necessary to determine the required stone size, thickness, and filter stability. An overview of existing design criteria and approaches is given by De Vos (2008) and De Vos et al. (2011). In addition, De Vos et al. (2012) derived a dynamic approach for the design of scour protection, which allows limited movement of top-layer stones for certain sea conditions. Furthermore, Whitehouse et al. (2011) compared and analyzed the application of scour protection in several offshore windfarms. A comprehensive summary of research on scour development is given by Sumer et al. (2001) and a recent review of numerical as well as physical modeling of scour and scour protection is presented in Sumer (2014). The selection of the required stone size is still usually based on amplification factors around foundation structures and the criteria of the threshold of motion by applying the classical Shields (1936) approach. This approach, however, neglects some characteristic properties of wide-graded material such as special grain size distribution and connected self-stabilizing effects under current load. These processes include the hiding effect, which describes the shielding of finer fraction by coarser grains and the exposure effect, which depicts the erosion of larger fraction due to its exposed and instable placement in the bed. As a consequence of these effects, larger fraction will be eroded at smaller shear stresses, and finer fractions need higher shear stresses for mobilization in comparison with a uniform sediment bed (Shvidchenko et al. 2001).

¹Research Associate, Franzius-Institute for Hydraulic, Estuarine and Coastal Engineering, Leibniz Univ. Hannover, 30167 Hannover, Germany (corresponding author). E-mail: schendel@fi.uni-hannover.de

²Senior Research Associate, Franzius-Institute for Hydraulic, Estuarine and Coastal Engineering, Leibniz Univ. Hannover, 30167 Hannover, Germany; Dept. of Civil Engineering, Univ. of Ottawa, Ottawa, ON, Canada K1N 6N5.

³Managing Director and Chair, Franzius-Institute for Hydraulic, Estuarine and Coastal Engineering, Leibniz Univ. Hannover, 30167 Hannover, Germany

Note. This manuscript was submitted on October 20, 2014; approved on July 9, 2015; published online on December 30, 2015. Discussion period open until May 30, 2016; separate discussions must be submitted for individual papers. This paper is part of the *Journal of Waterway, Port, Coastal, and Ocean Engineering*, © ASCE, ISSN 0733-950X.

Furthermore, the selective erosion of finer fractions leads to the coarsening of the bed surface and the development of an armor layer. However, scour protection around a structure is subject to a turbulent flow field (Sumer and Fredsøe 2002) and oscillating vertical movement. Although finer fractions could be similarly washed out as a result, the stability behavior might be different from that under undisturbed flow conditions including hiding and exposure processes. The detailed knowledge of the behavior of wide-graded material applied in a single-layer scour protection is particularly important for a dynamic design (De Vos et al. 2012) that allows the limited erosion of material for certain sea states.

The direct influence of sediment nonuniformity on local scour depth around piers under clear-water conditions was investigated by Ettema (1976). Additionally, Chiew (1984) and Baker (1986) (also presented in Melville and Sutherland 1988 and Sumer and Fredsøe 2002) performed studies with live-bed conditions. These studies showed a clear reduction of the local scour depth with increasing sediment nonuniformity (represented by the geometric standard deviation σ_g) due to the armoring and self-stabilizing effects. The results demonstrate the significance of sediment gradation on scour development, especially under clear-water conditions.

Therefore, numerous studies were performed to extend Shields approach regarding the fractional incipient motion for nonuniform sediments (e.g., Egiazaroff 1965; Ashida and Michiue 1971; Parker et al. 1982b; Andrews 1983; Kuhnle 1993; Wu et al. 2000). While Kuhnle (1993) performed laboratory experiments with several different gravel and sand mixtures, Parker et al. (1982b) used field data as the basis for the definition of a critical condition for incipient motion of nonuniform sediments. Andrews (1983) determined fractional critical shear stresses for nonuniform bed materials based on extensive bed load transport measurements in three rivers with naturally sorted gravel and cobble bed material. Finally, Wu et al. (2000) established an approach that predicts the probabilities of hiding and exposure effects among particles in the bed surface. The approach was verified by comparison with laboratory data and measurements of riverbed loads. Since these studies were focused on fluvial erosion and sedimentation processes, the established approaches are limited to the specific sediment properties and flow conditions, which are common in hydraulic engineering applications.

The aforementioned innovative, wide-graded quarry-stone mixture varies in grain size distribution from previously investigated materials. The grain size distribution was designed to fulfill the geotechnical and hydraulic filter requirements, making the installation of an additional filter obsolete. The characteristics of this kind of material are illustrated by the grain size distributions of the material samples tested in this study. In addition, hydraulic conditions need to be expanded to estuarine and coastal conditions. For the material under investigation no suitable approaches exist so far. Common approaches for the incipient motion of nonuniform materials cannot be directly applied to wide-graded quarry-stone materials. Consequently, extensive large-scale hydraulic model tests were performed at Franzius-Institute for Hydraulic, Estuarine and Coastal Engineering, Leibniz University Hannover, Germany, to investigate the stability of wide-graded materials under estuarine and marine wave and current conditions. The model tests aimed at advancing principle knowledge and physical properties of extreme wide-graded material and defining safer and more economic design criteria for scour and bed protection systems. A two-phase test program involved the determination of erosion stability and the assessment of the potential as scour protection, particularly in a dynamic design, of wide-graded quarry-stone material under (1) unidirectional flow conditions and (2) spectral wave load (Schendel et al. 2014).

This paper focuses on the first part of the test program and describes the required state of the art in the next section. The following sections outline the experimental design and procedures and present the applied analysis methods. Then, the assessment of erosion stability under steady flow conditions is given by outlining the displacement processes of the bed and determining fractional incipient motion and reviewing the applicability of established approaches for erosion stability of nonuniform sediments. Finally, the results are discussed.

State of the Art

Shear Stress Estimations for Rough Beds

As pointed out recently by Bagherimiyab and Lemmin (2013), local estimates of shear stresses in fully rough flows may strongly deviate from the common shear stress approach for uniform open-channel flows, i.e., $\tau_o = \rho g R I$, with τ_o as the bed-shear stress, ρ as the fluid density, g as the gravitational acceleration, R as the hydraulic radius, and I as the bed slope. Because of the nonuniformity of the flow, as a consequence of the bed roughness, strong pressure variations may be caused in the near bed region. It is therefore recommended to conduct detailed flow measurements to estimate the bed-shear stress correctly, which can either be accomplished with direct or indirect measuring devices. Since the application of direct methods is often not feasible due to heterogeneity of the surface and a resulting strongly fluctuating shear stress distribution along the surface, shear stresses in the vicinity of rough beds are mostly determined by indirect approaches. The latter are generally referred to as shear stress estimations, and they regularly rely on near bed velocity and turbulence measurements.

Due to the still existing uncertainties regarding the thickness of the roughness layer (Bagherimiyab and Lemmin, 2013) and the determination of the actual zero bed level for rough beds, in such contexts the measurement of the horizontal velocity over the depth of the water column should be preferred over single point measurements, since supplementary information about the flow characteristics and therefore roughness layer are provided (Bagherimiyab and Lemmin 2013; Rowinski et al. 2005). An often applied method (e.g., Wilcock 1996; Petrie et al. 2010) to estimate the bed-shear stress takes the logarithmic law into account, which is expressed as

$$\frac{u}{u_*} = \frac{1}{\kappa} \ln\left(\frac{z}{z_0}\right) \quad (1)$$

where the shear velocity u_* is defined as $u_* = \sqrt{\tau_o/\rho}$; u is the velocity at height z above the bed; z_0 is the bed roughness length; and κ the Karman-Constant with $\kappa = 0.4$.

With available velocity profiles, a least-square approach can be used to fit the logarithmic profile to the data. While this method yields some inaccuracies in the fitting (Biron et al. 2004), it has the notable advantage of providing the required roughness length for each profile (Petrie et al. 2010).

Where the technical requirements for turbulence measurements are given, the bed-shear stresses can equally be estimated on the basis of the Reynolds stresses $\overline{u'w'}$, with u' and w' as the velocity fluctuations of the streamwise component u and the vertical velocity component w . In a two-dimensional (2D) uniform flow, the bed-shear stress can be obtained by extrapolating the nearly linear distribution of the Reynolds stresses over the water depth to the bed (Nikora and Goring 2000; Bagherimiyab and Lemmin 2013). Similar to the Reynolds stress approach, the turbulent kinetic energy (TKE) method is also based on turbulence measurements,

yet using the turbulent velocity components of all three flow directions (Biron et al. 2004). The TKE is defined as $k = 0.5 (\overline{u'^2} + \overline{v'^2} + \overline{w'^2})$ and the bed-shear stress can be calculated by the relation $\tau_0 = C_1 \rho k$, with C_1 as a proportionality constant. The value $C_1 = 0.19$ was used by Rowinski et al. (2005) for rough bed open-channel flow with satisfactory results.

Further methods for an estimation of bed-shear stresses based on velocity and turbulence measurements are compared in Kim et al. (2000), Biron et al. (2004), Rowinski et al. (2005), or Bagherimiyab and Lemmin (2013). Their studies have indicated that the applicability of these methods is strongly influenced by the present flow and roughness conditions; therefore the comparison of several methods seems advisable for a reliable estimation of bed-shear stresses.

Incipient Motion of Wide-Graded Sediment under Current Conditions

To define the incipient motion of nonuniform sediment mixtures, additional self-stabilizing processes have to be taken into account compared with uniform sediment. These processes include a so-called hiding process, which describes the covering of finer fractions from the flow by larger fractions and, vice versa, the so-called exposure process. The latter process refers to the erosion of larger grain size fractions in a given flow condition as a consequence of their exposed placement on the bed, i.e., well above the average bed level. As a result, finer fractions in a wide-graded sediment bed may demand a significantly higher critical shear stress to be mobilized compared with a similar grain size uniform sediment bed. On the contrary, larger fractions could be eroded at lower critical shear stresses (Shvidchenko et al. 2001). To adapt critical shear stresses for specific fractions of a mixture in comparison with uniform sediments, hiding functions are generally implemented to describe how incipient motion for grain sizes in certain mixtures deviates from those of uniform beds. The prediction of the incipient motion of nonuniform sediments has been established in numerous studies for different sediments and test conditions (e.g., Egiazaroff 1965; Ashida and Michiue 1971; Hayashi et al. 1980; Parker et al. 1982b; Andrews 1983; Carling 1983; Kuhnle 1993; Wilcock 1993; Wu et al. 2000; Patel et al. 2014). Generally these approaches relate the specific fraction d_i of the sediment mixture to a reference size fraction d_R , often the median grain diameter d_{50} , and are expressed as

$$\frac{\tau_{c,i}^*}{\tau_{c,R}^*} = f\left(\frac{d_i}{d_R}\right) \quad (2)$$

$$\tau_{c,i}^* = \frac{\tau_{c,i}}{(\rho_s - \rho)gd_i} \quad (3)$$

$$\tau_{c,R}^* = \frac{\tau_{c,i}}{(\rho_s - \rho)gd_R} \quad (4)$$

where $\tau_{c,i}$ is critical shear stress of the considered fraction d_i ; $\tau_{c,R}$ is the critical shear stress of the reference size fraction d_R ; ρ_s and ρ are the specific densities of the sediment and water; and g is the gravitational acceleration.

Wilcock (1988) categorized two methods for an estimation of the critical shear stress $\tau_{c,i}$. The first method contains the definition of a reference transport rate (reference transport method, RTM) at which a certain amount of a fraction will be transported (e.g., Parker et al. 1982b; Kuhnle 1993; Shvidchenko et al. 2001). The measured transport rates of individual fractions are plotted against

corresponding shear stresses. On the basis of a predefined reference transport rate the critical shear stress for the measured fractions can be determined. A dimensionless criterion for the fractional reference transport rate is defined by Parker et al. (1982b) as

$$W_i^* = \frac{\left(\frac{\rho_s}{\rho} - 1\right) g q_{si}}{\rho_s u_*^3 f_i} \quad (5)$$

where ρ_s is the sediment density; q_{si} is the sediment transport rate for the fraction i ; u_* is the shear velocity; and f_i is the proportion of fraction i in the bed material. Parker et al. (1982b) suggested a small reference transport rate of $W_i^* = 0.002$ for the application of the RTM.

By a second method, as categorized by Wilcock (1988), the critical shear stress $\tau_{c,i}$ can also be estimated by the largest transported fraction (largest-grain method, LGM), which is measured either by bed load samples or by visual observations (Andrews 1983; Carling 1983, Komar 1987). This way the largest measured fraction can be used directly as a critical condition for the incipient motion, as long as coarser fractions are still available in the bed.

A reliable application of the reference transport method requires a sufficient number [Wilcock (1988) suggested 5–10] of transport samples for different flows to assure an accurate definition of the relation between shear stress and transport rate. In return, the results obtained with the largest-grain method may be affected by sampling and scaling problems, as it often cannot be guaranteed that the largest possible fraction in motion is captured, particularly in field measurements. Furthermore, Wilcock (1988) pointed out that a direct comparison between the critical shear stress estimations by the two methods may be difficult, because the considered transport sample is very different. Whereas the largest-grain method refers to a single largest grain, the reference transport method applies to all fractions within several transport samples.

Previous Work

Incipient motion and sediment transport are important aspects in hydraulic and coastal engineering. This is reflected by the large number of past studies on erosion stability of uniform and graded sediments. Since the Shields approach is still the most widely used entrainment criterion for uniform sediments, recent studies concerning uniform sediments often focus on an improvement or an assessment of the conventional Shields approach regarding the particle entrainment for specific applications. Coleman and Nikora (2008) presented a new unifying framework for particle entrainment by using general equations for fluid motion and particle stability. They found that, among others, bed-shear stresses and sediment bed characteristics are key parameters regarding the hydrodynamic particle entrainment. To simplify the application of the Shields diagram, Cao et al. (2006) derived an alternative formulation by deploying a logarithmic matching method, enabling the determination of the Shields parameter directly from fluid and sediment characteristics.

In addition to uniform cohesionless sediments, the critical shear stress of cohesive sediments is given attention in other studies. Kothiyari and Jain (2008) investigated the influence of cohesion on the incipient motion of sediment mixtures consisting of sand, gravel, and clay proportions. Based on their experiments, they proposed a relationship for the determination of critical shear stress for cohesive as well as for cohesionless sediment mixtures. They found that, depending on the percentage of clay within the sediment mixture, the ratio of critical shear stress for cohesive sediment to the critical shear stress for the equivalent cohesionless sediment can be more than 3.

In view of nonuniform sediments the suitability of earlier approaches for the determination of incipient motion of graded or bimodal sediment mixtures is taken into focus in newer studies. The results of Patel and Ranga Raju (1999) and Patel et al. (2013, 2014) showed that approaches based on the median grain diameter as reference size are less accurate for the determination of fractional critical shear stress for nonuniform sediments. To account for the characteristics of graded sediments, they proposed a relationship that contains the geometric standard deviation σ_g within the reference size.

Despite the numerous studies on nonuniform sediments many coastal sediment transport formulas (e.g., van Rijn 1993; Ribberink 1998) assume uniform sediments. So far, only a relatively small number of studies have considered the transport of nonuniform sediment both under current and wave conditions in coastal areas. Among these is van Rijn (2007), who extended his own attempts of bed load and suspended load transport model (van Rijn, 1993) in river flow to oscillatory flows and currents in coastal waters. The model can be applied only to finer grain sizes in the range from 8 to 2,000 μm . Furthermore, Wu and Lin (2014) developed combined formulations on bed load and suspended load transport under non-breaking waves and currents. Based on the approach of Wu et al. (2000) hiding and exposure mechanisms in nonuniform sediments were considered in their attempts.

However, the incipient motion of wide-graded, broken stone material has not been examined extensively. Available approaches for incipient motion and transport of nonuniform and graded sediments are clearly limited to properties of natural fluvial and coastal sediments. Therefore the underlying key processes of armor layer development in broken stone materials is still unclear, and to what extent the characteristic hiding and exposure effects have to be considered regarding the definition of the fractional initiation of motion for the stability design of granular scour and bed protection systems is unresolved.

To address this knowledge gap, hydraulic model tests have been performed to investigate the armor layer development of wide-graded quarry stone under unidirectional flow and to assess the stability of this material with respect to the fractional critical shear stress of nonuniform sediments.

Experimental Setup

The hydraulic model tests were performed in the closed-circuit flume of the Franzius-Institute for Hydraulic, Estuarine and Coastal Engineering, Leibniz University Hannover, Germany. Detailed information and technical drawings of the flume can be found in Goseberg et al. (2013). In addition to their experimental setup, the artificial ramp was removed so that a horizontal bottom could be used in the tests. Groins and a flow straightener were installed upstream of the sediment pit to reduce the influence of the flume bend on the lateral velocity distribution.

The model tests were performed in a scale of 1:1 to avoid scaling effects that could particularly bias the behavior of finer sediment fractions in the tested sediment mixture. The applied wide-graded material was installed in a deep pit with a width of 1.0 m, a length of 2.7 m, and a depth of 0.6 m resulting in a specimen surface of 2.7 m^2 . The material was built in at the level of the flume bed in a thickness of 200 mm (corresponds to the maximum grain diameter) without further compaction. In reference to the available maximum flow velocities in the flume and as a requirement for the largest-grain method, the movement of the largest grains, i.e., 200 mm, was not anticipated or observed during the experiments. The depth of the material layer should be enough to guarantee an unaffected

erosion of finer fractions, particularly since the median diameter (~ 50 mm) is far smaller than the depth of the material layer. To ensure a good interlocking with the subsurface, an additional material layer was placed under the material bed. This sublayer consisted of the same wide-graded material with a grain size distribution similar to the investigated material, but from a different sample. In contrast to the investigated material on top, the sublayer has not been removed during the experiments. Information of the experimental setup in the circulation flume is illustrated in Fig. 1.

Instrumentation

To determine the changes of the bed topography over time and to identify erosion and deposition areas on the rough bed after flow exposure, digital elevation models (DEMs) of the bed topography were measured with a laser distance sensor (OADR 2016480, Baumer, Friedberg, Germany; resolution 0.015–0.67 mm). A vertical accuracy of approximately 1.0 mm was achieved by calibration in preliminary tests and subsequent error correction.

The eroded bed load fractions have been collected by an adjacent sediment trap, which was placed 6.0 m downstream of the sediment bed (Fig. 1). For constructional reasons the sediment trap was designed as an artificial pit trap above the concrete flume bottom, consisting of a container with flat slopes on both ends. The sediment trap had a total length of 0.8 m and spans the whole flume width. Suspended material was not measured by the sediment trap. Apart from obtaining the amount of eroded material, the grain size distribution of the eroded bed load was determined for each test run.

To estimate bed-shear stresses in accordance with the findings from a literature search, three-dimensional (3D) velocity measurements were performed by an acoustic Doppler velocimeter (ADV) (Vectrino+, Nortek, Rud, Norway). A sampling rate of 200 Hz and a measuring period of 30 s for each position were determined to be a fair balance between the amount of recorded data and repeatability. Because of the exceptionally rough surface structure (maximum grain diameter is 200 mm) the horizontal and vertical positions of the ADV device and the number of the velocity measurements had to vary between the experiments. To ensure comparable velocity measurements, the measurement positions were arbitrarily determined on the basis of similarity of surface formations in the given bed surface (e.g., near large single grains or in the vicinity of hiding structures). In combination with the collected bed load, the shear stress estimates provided the basis for the definition of an initial-motion criterion and the possibility to assess the erosion stability of the material. To position the laser distance sensor and the ADV probe automatically and reproducibly, a three-way traverse system was installed over the sediment bed (Fig. 1). By using this system, the bed topography could be scanned in a gridlike pattern and the velocity measurements could be done at predetermined positions for the series of load cases within single test runs.

Description of Wide-Graded Quarry-Stone Material

The applied material was a wide-graded quarry-stone mixture made of granodiorite with a grain size distribution in the range of 0.063–200 mm. Material samples were obtained by the manufacturer on the basis of wheel-loader-filled big bags with volumes of approximately 1 m^3 each. Fig. 2 presents the grain size distributions of the three individual samples, which were obtained from site analysis of the individual big bags. The analysis of the three samples showed significantly varying grain size distributions, which stressed the necessity for experimental repetition to guarantee reasonable reproduction and to account for the inherent uncertainties within the

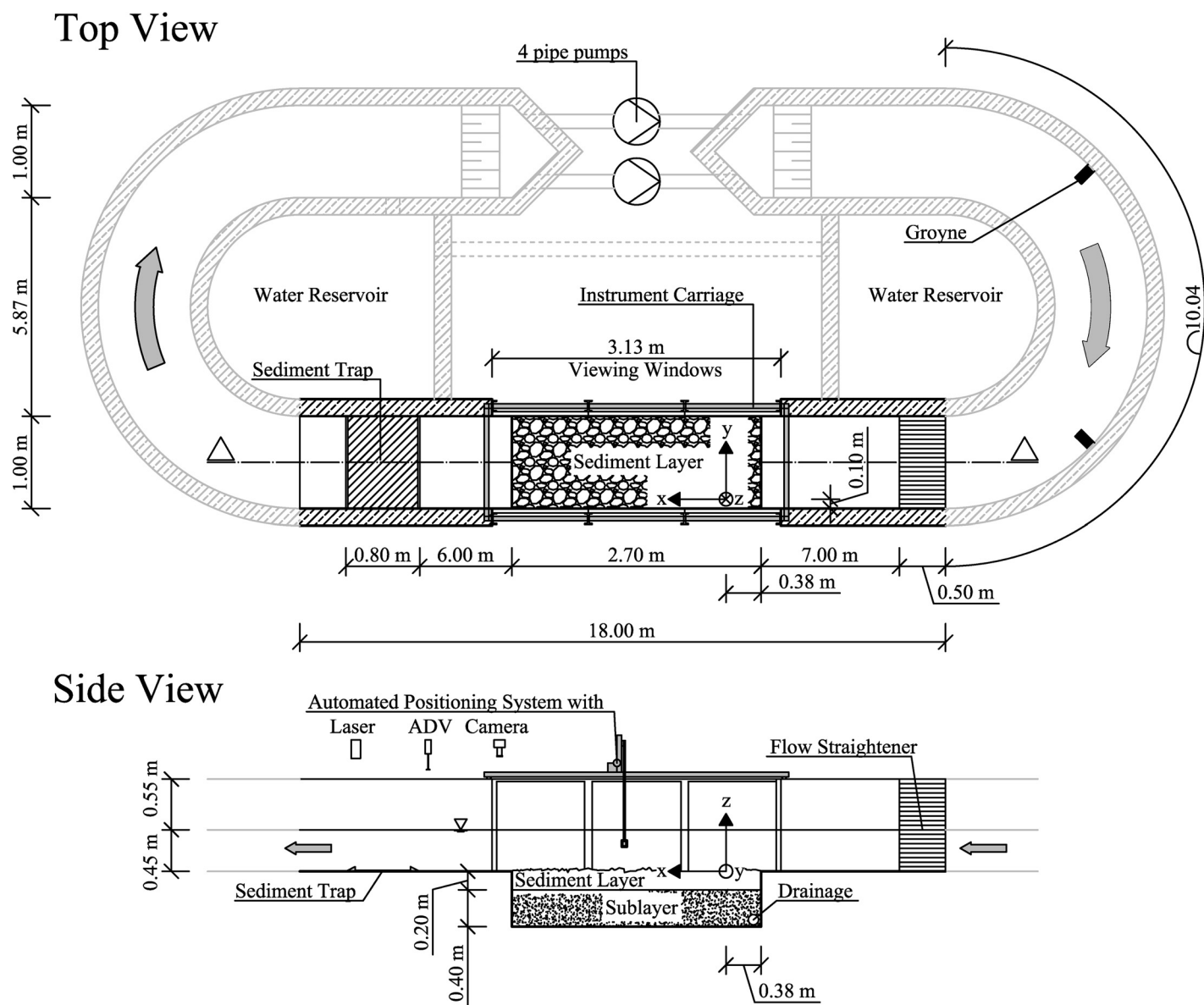


Fig. 1. Schematics of experimental setup in top and side views (not to scale)

wide-graded material properties. Table 1 summarizes the grain size and gradation characteristics of the three material samples.

Experimental Procedure

To guarantee the reproducibility of the results, a series of three repeating experiments were accomplished. Each experiment consisted of seven load cases, with successively increasing mean flow velocities from 0.1 to 0.9 m/s (see Table 2). Mean flow velocities \bar{u} were determined in preliminary tests without a sediment bed and represent the mean flow velocities averaged over a cross-sectional area at the inspection window. Exemplarily, Fig. 3 shows the distribution of streamwise flow velocities over the flume width for the highest load case ($\bar{u} = 0.9$ m/s). A slight nonuniformity of the flow between the outer (left) and inner (right) wall of the circulation flume is evident. Although the pattern of the streamwise nonuniformity is also present for slower velocities, the magnitude of differences between the inner and outer flume wall is smaller. Goseberg et al. (2013) found the influence of the nonuniformity negligible and verified the general suitability of the circulation flume for the

generation of long waves. The generated waves mimicking tsunami had effective periods of up to 120 s and the associated flow comprising the wave motion exhibited current characteristics. Their conclusion about the negligibility of the nonuniformity also applied to the described experiments. However, the formation of such nonuniformity should be prevented by the experimental setup. Using a new tilting flume, the nonuniformity will be accounted for in future studies.

The duration for each load case T was at least 2 h, so that a cumulated exposure time of 14 h for each experiment was obtained. In each experiment a different material sample from the same wide-graded material was used (see Table 1).

At the beginning of the experiments water was carefully filled in from both sides of the material bed to avoid unwanted washout effects of the finer fractions. No additional sediment was added to the flume upstream of the test bed during the experiments; however, minor amounts of suspended sediment were recirculated with the temporarily stored flume water due to the closed system of the flume. Subsequent to each load case the water was carefully drained to allow an undisturbed measurement of the bed surface

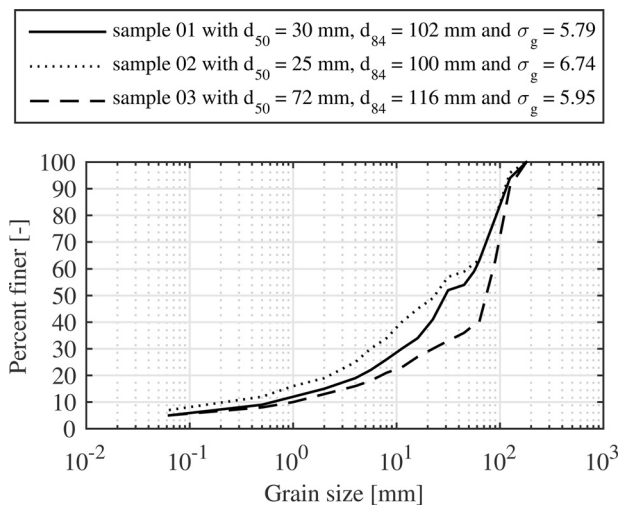


Fig. 2. Grain size distributions of investigated wide-graded material samples

Table 1. Grain Size and Gradation Characteristics of Material Samples

Sample	d_{10} (mm)	d_{16} (mm)	d_{30} (mm)	d_{50} (mm)	d_{60} (mm)	d_{84} (mm)	C_u (-)	C_c (-)
01	0.6	2.5	11.2	30	62	102	103	3.37
02	0.4	1.0	5.6	25	56	100	140	1.40
03	1.0	4.0	22.4	72	85	116	85	5.90

Table 2. Load Cases and Corresponding Mean Flow Velocities \bar{u} for All Experiments

Load case	\bar{u} (m/s)
1	0.1
2	0.18
3	0.24
4	0.38
5	0.56
6	0.72
7	0.9

Note: \bar{u} is the mean flow velocity averaged over a cross-sectional area during preliminary tests without sediment bed.

by the laser scanner and to extract the eroded material from the sediment trap.

During the experiments the flow velocity over the sediment bed was measured at five positions along the longitudinal axis of the flume. These positions were kept fixed over all load cases within one experiment to ensure the comparability of the measured flow velocities. In addition, further positions for velocity measurements were chosen dependent on characteristic formations within the surface structure, in particular hiding and exposure areas. These additional positions changed between the individual experiments but remained the same during a single experiment. The positions of the measurement points are highlighted in the DEMs presented in Fig. 4. At each of the positions a velocity profile was measured and resolved by eight points over half the water depth. The distances between the eight points were fixed throughout all experiments with 1 cm for the five points closest to the bed and 5 cm for the remaining three points. The distance of the point closest to the bed varied due to the very irregular surface structure of the sediment bed and due to

the sediment displacement during the experiment. Since this distance between the closest measurement location and the specimen surface is very important for the determination of the correct bed-shear stress, it was determined by a built-in bottom check of the ADV probe for every position and load case. All velocity measurements were performed at the end of the individual load cases after a stable bed was developed and sediment transport could no longer be observed. It should be noted that, as a result, a potential change of the flow field due to erosion and increasing bed roughness during loading could not be considered. Table 3 summarizes the test parameters and conditions for the accomplished erosion tests for wide-graded quarry-stone mixtures.

The scan area recorded by the laser distance sensor covered 60% of the total surface of the sediment bed as shown in Fig. 5. The reduction of the scan area was performed so that neither scour, due to bed roughness changes at the interface between test specimen and concrete channel bottom, nor wall effects had a negative influence on the bed topography transformation. The fact that only a part of the bed topography is measured by the laser scanner should be considered in case of a comparison between the measured amount of eroded bed load by laser scanner and sediment trap.

The bed topography was scanned in longitudinal profiles with a sampling interval of $\Delta x = 0.5$ mm and a lateral spacing of $\Delta y = 5$ mm. A theoretical vertical resolution between 0.015 and 0.67 mm is given by the manufacturer, depending on the measurement distance. In total, the bed topography is covered with 160 profiles and over 630,000 individual measurement points for each scan. Along with a reference scan at the beginning of an experiment and with a laser scan subsequent to each load case, eight laser scans were conducted for each experiment.

The sediment trap was emptied after each load case. The eroded bed load was dried and the grain size distribution was obtained in accordance with engineering code DIN ISO 3310. Because of the small amount of eroded material in the first three load cases, a sieving in conformity to the aforementioned given standard could be achieved for Load Cases 4–7 only. The obtained grain size distributions were compared among themselves and with the initial bed material of the used material samples. Characteristic grain sizes, e.g., d_{50} , d_{84} , d_{90} , were calculated.

Applied Analysis Methodology

Analysis Methods

Subsequent to the elimination of occasional spikes in the laser sensor signal due to incorrect backscatter of the signal, the point cloud from laser measurements was interpolated to a 1×1 -mm grid accomplished by a cubic Delaunay triangulation to generate detailed DEMs. By calculating the elevation differences between the DEMs through subtraction of the individual load cases, erosion and accumulation areas within the bed surface are present and a volumetric determination of displacement processes were determined. To account for measuring inaccuracies in terms of additional settlement or unavoidable signal noise of the laser sensor, only elevation differences greater than ± 2 mm were considered. This threshold was obtained by test measurements and sensitivity studies. The sensitivity studies included multiple scans of the same bed topography. On average, 90% of the measured differences were located under the threshold of ± 2 mm. Here, it has to be taken into account that some larger differences were based on offsets at the edge of large stones and therefore could not be eliminated by choosing a reasonable threshold value. Subsequently, the sensitivity of the amount of transported sediment to several threshold values was determined.

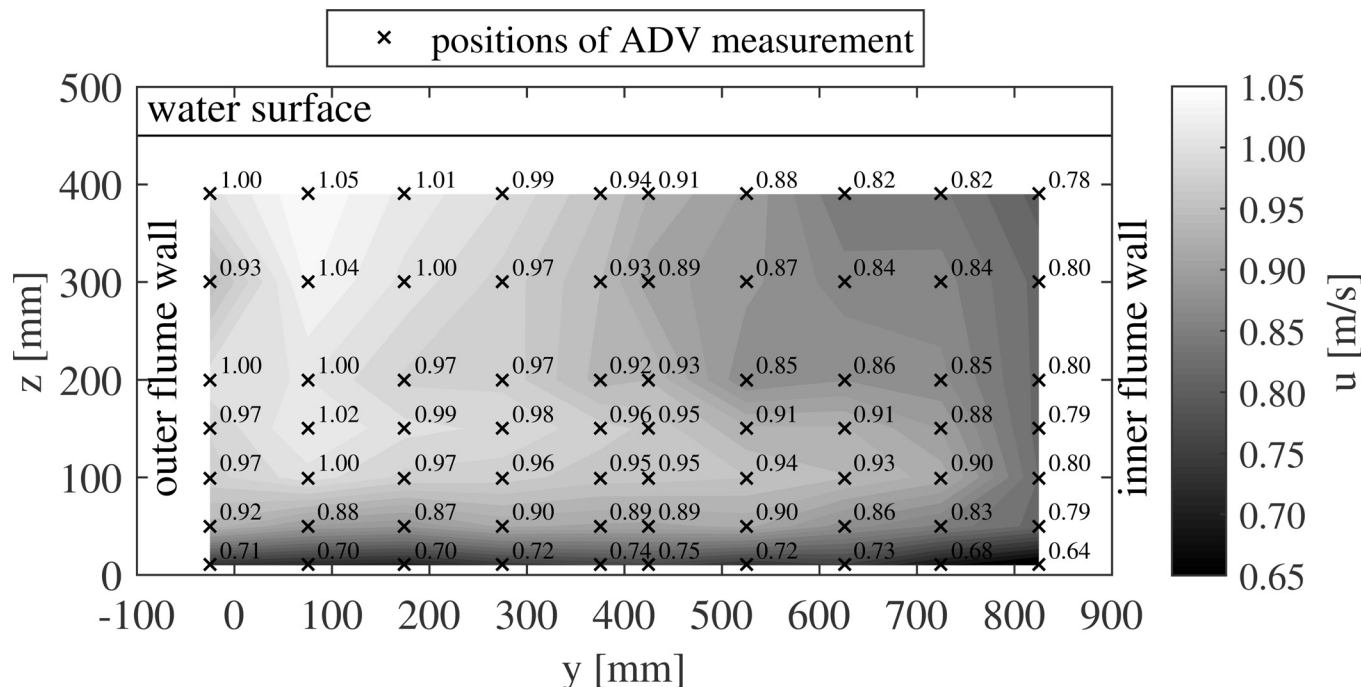


Fig 3. Distribution of time-averaged flow velocities in meters per second over the flume width y during preliminary testing for the highest load case (mean $\bar{u} = 0.9$ m/s); the velocities were measured 1 m upstream of the sediment bed

Table 3. Test Conditions for All Three Experiments

Experiment	Sample	d_{50} (mm)	d_a (mm)	σ_g [-]	\bar{u} (m/s)	T (min)	H (cm)
A	01	30	48	5.79	0.10–0.90	120	45
B	02	25	44	6.74	0.10–0.90	120	45
C	03	72	66	5.95	0.10–0.90	120	45

Note: T is the duration of a single load case; H is the water depth above the material bed.

For the chosen threshold of ± 2 mm only a potential reduction of 5% of the transported sediment volume was calculated on average, which was considered acceptable.

Fig. 4 shows the DEMs of the reference scans in the beginning of each experiment. Even though the same wide-graded material was utilized to obtain the tested material samples, significant differences in surface structure and roughness are evident between the experiments as presented in Fig. 4. The mean bed elevation above the flume bottom varies between the three experiments with $z_{\text{mean}} = 27.47$ mm for Experiment A, $z_{\text{mean}} = 49.76$ mm for Experiment B, and $z_{\text{mean}} = 46.23$ mm for Experiment C. The parameter z_{mean} represents the mean value of all bed elevations saved in the DEMs relative to the level of the flume bed and additionally illustrates the differences in the installation height between the experiments.

Based on the ADV measurements the bed-shear stresses were determined. The signal processing contained spike elimination and noise reduction. Furthermore, the flow velocity was averaged over 30 s for each measurement point. The bed-shear stresses were estimated on the assumption of a logarithmic velocity distribution within the boundary layer [Eq. (1)] as applied in, e.g., Biron et al. (2004) and Petrie et al. (2010). The log law method was given the preference over turbulence-based methods (i.e., Reynolds and TKE), even though it would have been possible to obtain

turbulence data from the 3D velocity measurements. This is partially due to the limited resolution of the measured velocity profile resulting from internal time constraints and because a reasonable and consistent distribution of Reynolds or TKE stresses over the water depth could not be achieved in the cases reported herein. Furthermore, as a result of the nonuniformity of the flow, which is further amplified by the inhomogeneous bed surface, an assumption of an almost linear distribution of the Reynolds or TKE shear stresses, which would hold true for a strict 2D uniform flow, is associated with noteworthy uncertainties. Fig. 6 shows the measured velocity profiles for Experiment B in the end of Load Case 7 and compares a measured velocity profile with the log law [Eq. (1)] to provide a mean to evaluate the accuracy of the approach. While the velocities corresponded reasonably with the log law in the logarithmic region, they deviated from the log law in the outer region ($z/H > 0.2$), as expected.

The log law method requires the knowledge of the present bed roughness, i.e., the roughness length z_0 . Due to the wide-graded material properties and thereby the inhomogeneous bed surface, a global roughness length depicts an inappropriate mean for all measurement positions. By measuring velocity profiles and fitting a logarithmic equation in the form of $\ln z$ to them, local roughness lengths for each measurement position can be determined instead. The fitting is performed by using a least-square error approach. The goodness of fit can be measured by the coefficient of determination R^2 . In consideration of the existing flow conditions a relative good fitting quality $R^2 > 0.91$ combined for all positions could be achieved. For further analysis and the calculation of the bed-shear stresses only profiles with $R^2 > 0.85$ were applied, which was the case for 194 of the total 224 velocity profiles. On the basis of the log law [Eq. (1)], the roughness length z_0 can be calculated by

$$z_0 = \left(z_1 z_2 \frac{u_1}{u_2} \right)^{\frac{u_2}{u_2 - u_1}} \quad (6)$$

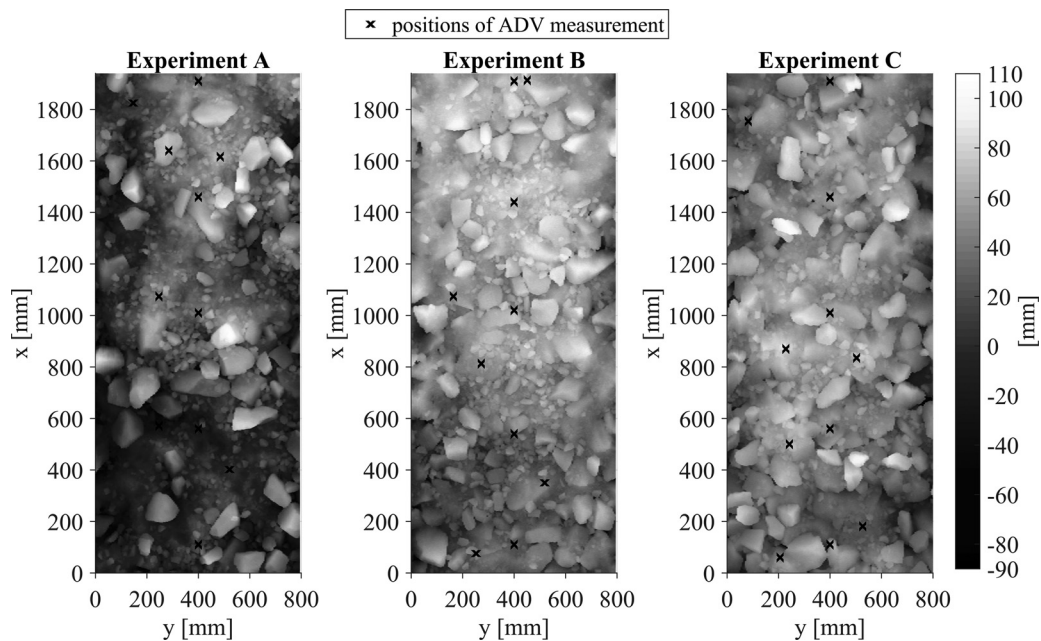


Fig. 4. Digital elevation models of initial bed surface for the three experiments; flow direction is from the bottom to the top

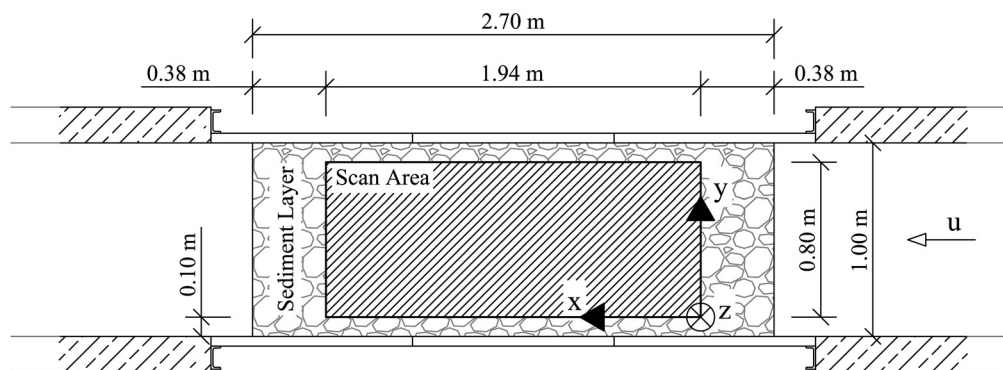


Fig. 5. Bed surface area covered by the laser scanner (1.55 m^2) in relation to the total dimensions of the material bed (2.70 m^2)

with u_1 and u_2 as the velocities at the bed-nearest positions z_1 and z_2 . As a consequence of the inhomogeneous bed and the progressing erosion of the bed, the distances z_1 and z_2 as well as the corresponding velocities u_1 and u_2 vary heavily between the measurement points (Fig. 4) and with increasing loading. Exemplarily, Table 4 shows values for these parameters for Experiment B.

Subsequently, the shear velocity and local bed-shear stresses were calculated using [Eq. (1)]. Fig. 7 shows the distribution of mean bed-shear stresses $\bar{\tau}_0$, which are the averaged shear stresses over all positions for a specific load case and the standard deviations for all experiments in reference to mean flow velocity. While the bed-shear stresses for the individual experiments are quite similar for a certain flow velocity, the shear stress variations caused by the inhomogeneous bed and the resulting turbulence are obvious and underline the need for several different measurement positions to get an sufficient overview of existing bed-shear stresses.

Fractional Critical Shear Stress

The assessment of the erosion stability of the investigated material was based on the determination of fractional critical shear stress as

a condition for the incipient motion. Because of the relative small amount of available load cases with sufficient transport rates, a meaningful relation between the obtained bed-shear stress and the transport rate of available sediment fractions could not be defined. Instead, the comparison of the calculated bed-shear stresses with representative grain sizes from the sediment trap is applied as critical condition for incipient motion. Here, the largest grain fraction collected by the sediment trap and determined by sieve analysis was considered as critical grain size in accordance with the largest-grain method. In each experiment and load case coarser fractions were still available in the bed as a consequence of the wide-graded material properties with grain sizes up to 200 mm. However, the grain size distribution could be determined only for the last four load cases in each experiment; therefore, only for these load cases could the largest grain size be defined. Table 5 summarizes the mass of bed load collected by the sediment trap, illustrating the significant differences of erosion between the three experiments. The amount of collected bed load correlates with the amount of finer fractions in the three material samples (cf. Fig. 2). Therefore, differences in bed surface structure (see Fig. 4) as well as in the initial material distribution should be considered in the analysis of the results.

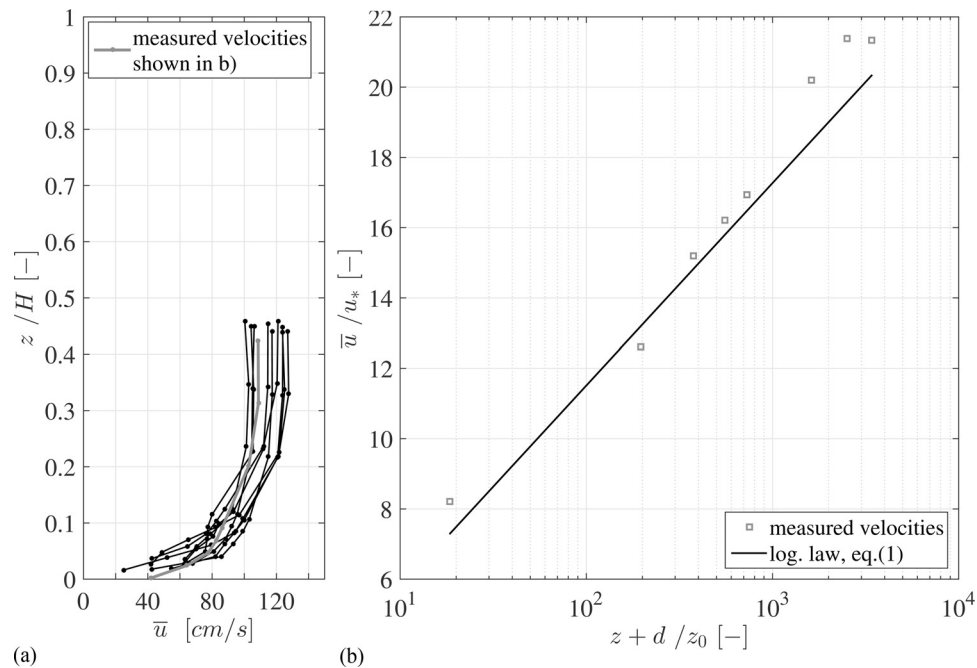


Fig. 6. (a) Distribution of time averaged horizontal velocities for Experiment B in the end of Load Case 7, measurement positions are shown in Fig. 4; (b) comparison of measured velocities [gray profile in (a)] and log law; u_* and z_0 are calculated by applying a logarithmic fit to the measured velocity profiles, the vertical displacement is $d = 0.25(k_S/3)$ with $k_S = 30z_0$

Table 4. Exemplary Values for the Measurement Distance z_1 and z_2 to the Bed and the Measured Corresponding Velocities for Experiment B

Load case	z_1 (cm)	z_2 (cm)	u_1 (m/s)	u_2 (m/s)
1	0.9	1.9	0.049	0.058
2	1.0	2.0	0.103	0.104
3	1.4	2.4	0.161	0.185
4	0.7	1.7	0.262	0.312
5	0.9	1.9	0.392	0.455
6	2.1	3.1	0.545	0.627
7	1.6	2.6	0.424	0.648

In the following, the experimental results, which were obtained on the basis of the earlier outlined methodology, are presented and discussed.

Results

Bed Topography and Displacement Processes

During the experiments a significant coarsening of the bed surface at higher flow velocities has been observed by visual inspections. Particularly, the selective erosion of large quantities of the finer fractions rather quickly led to a coarsening of the bed at the beginning of each load case. Unfortunately, the amount of suspended material was not measured during the experiment and therefore no quantities can be given. The investigated material contained finer fractions, which would have been expected to be transported as suspended sediment. Surprisingly, only a modest turbidity of the water could be observed visually, despite the erosion of finer fractions at the beginning of each load case and the fact that the circulation flume is a closed system. Especially in the first three load cases, the

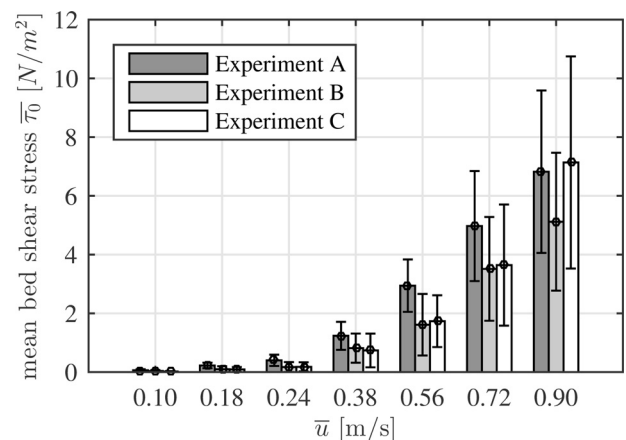


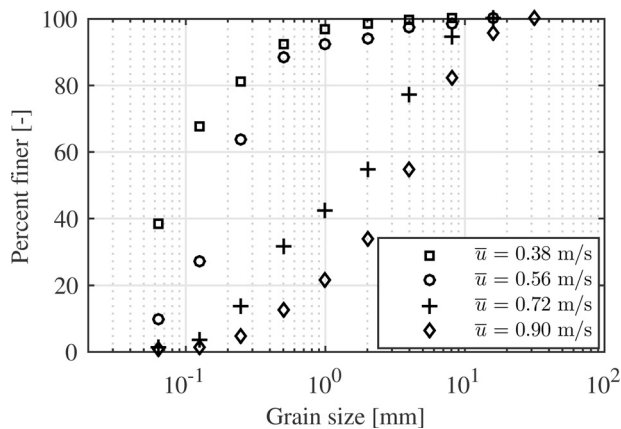
Fig. 7. Mean bed-shear stresses $\bar{\tau}_0$ and standard deviation $\tau_{0, \text{std}}$ of calculated bed-shear stresses for all experiments in reference to mean flow velocity \bar{u}

finer fractions clumped together and formed a dense surface structure. Because of occurring hiding processes, not all of the finer fraction was eroded, so that even in the highest load case, these fractions were available on the bed surface. In summary, the turbidity of the water and the amount of suspended load appeared to be unexpectedly small. Nevertheless, an unknown amount of material was eroded as suspended load and this has to be considered in the assessment of the sediment trap results. But given the fact that only a small amount of finer fractions was transported as suspended load, the estimation of critical shear stresses by the largest-grain method should not be affected.

With the removal of the test bed after the end of each experiment the formation of a very compact and tight grain structure was revealed, in which all fractions of the initial material were present.

Table 5. Mass of Bed Load Collected by the Sediment Trap after Each Load Case

Load case	Bed load		
	Experiment A (g)	Experiment B (g)	Experiment C (g)
1	—	—	—
2	—	—	—
3	—	—	—
4	59.6	292.0	362.6
5	146.6	244.3	214.7
6	265.7	542.4	177.7
7	852.5	1523.6	99.6
Σ	1324.4	2602.3	854.6

**Fig. 8.** Grain size distributions of eroded bed load collected by the sediment trap for the last four load cases in Experiment B

By the end of each load case sediment transport could no longer be observed. With the formation of a stable and immobile bed surface as indicators, the development of a static armor layer at the end of each load case can be concluded (Jain 1990; Marion and Fraccarollo 1997; Parker and Sutherland 1990). Due to the successive increase of flow velocities, the existing static armor layer was degraded at the beginning of each load case to develop a new one until the end of the respective load case. However, with the available velocities no sufficiently critical flow condition for a complete failure and destruction of the armor layer was achieved. Therefore, additional experiments with higher flow velocities are needed in the future for the determination of application-relevant load limits and definite assessment of the material performance.

The analysis of the sand trap results showed that in all experiments only grain sizes smaller than the d_{50} grain size of the initial bed were moved, which indicates relations of $d_i/d_{50} < 1$ for further analysis. The coarsening of the eroded bed load with increasing velocity is clearly observable for all experiments, indicating a continuously coarsening of the bed surface as well. Fig. 8 shows the development of the grain size distributions of the trapped bed load for Experiment B for the last four load cases. Based on the DEMs, plots of bed elevation differences between individual load cases were created, illustrating erosion and accumulation areas on the bed from sediment displacement processes. Figs. 9–11 show the displacement processes at the end of each experiment resulting from seven subsequently increased load stages after a total load exposure of 14 h. As expected, the erosion areas (dark gray) outweigh the accumulation areas (light gray). At the same time, erosion patterns occur

more globally distributed, reflecting areas with large quantities of finer fractions (dash-lined circles in Figs. 9–11), whereas accumulation is locally concentrated behind larger stones or similarly protected parts (full-lined circles in Figs. 9–11).

Erosion as well as accumulation areas and depth intensify with successively increasing flow velocities, especially for the last four load cases. As shown in Table 6 the mean erosion, averaged over the scan area, adds up to 1.4 mm for Experiment A, 3.6 mm for Experiment B, and 3.3 mm for Experiment C. Because of its heterogeneous appearance, this erosion should not be mistaken as a general lowering of the bed. Furthermore, the amount and the areas of erosion do not correlate with the streamwise nonuniformity of the flow over the flume width shown in Fig. 3. In Experiments B and C a large proportion of the erosion takes place on the inner side of the circulation flume, where the smallest velocities have been measured. For example, in Experiment B, while 47% of the total erosion volume was measured in the outer third of the flume width ($y = 0$ –266 mm) only 12% has been measured in the middle third and 41% in the inner third ($y = 524$ –800 mm). In addition to the streamwise velocities, lateral velocity components have been measured as well. This 3D behavior of the flow might be caused by a combination of aspect ratio of the channel (width/height = 2.22), secondary current, and roughness differences between wall and bottom. Since the lateral velocity components are small compared with the streamwise components (under 5% for the highest load case), it is unlikely that lateral velocity components are responsible for the erosion pattern. Therefore, it can be assumed that the distribution of the erosion over the sediment bed is more influenced by the inhomogeneous bed than by the nonuniformity of the flow.

Small movements of exposed larger stones transported along the test bed within the scanned area could even be identified by comparison of the DEMs. However, as those stones have not left the sediment bed, they were not considered as critical reference grain size for the incipient motion, but they still displayed the effects of exposure in nonuniform sediment beds very well. Also, Figs. 9–11 demonstrate the considerable differences in characteristic and quantity of erosion depending on initial grain size distribution, placement, and bed surface structure and illustrate the high uncertainty in relation to practical design.

To quantify the flow-induced changes of the bed surface, the development of the bed roughness with increasing velocities was also estimated by probability distribution functions (PDFs) of the bed elevations. The standard deviation of the bed surface elevation σ_z can thereby be interpreted as the characteristic, vertical roughness length of gravel beds (Marion et al. 2003; Aberle and Nikora 2006; Mao et al. 2011). To account for the initial slope of the bed (Fig. 4) and further changes of the bed slope during the experiments, the data were detrended in the streamwise direction using a linear interpolation. Subsequently, the PDFs were created by removing the mean bed elevations first and then plotting a smoothed histogram with 200 bins (Fig. 12).

Remarkably, the PDFs within an experiment show, with almost identical shape and distribution, no dependency on the applied flow velocities. However, the PDFs of the last load case for Experiments B and C show slightly smaller maximum probability densities in comparison with the initial bed, indicating an adjustment of the bed to increasing flow velocities, at least for the highest flow velocity of 0.9 m/s. Furthermore, the PDFs show a small peak for one of the loadings for each experiment. The load case for which the peak occurs varies between the experiments. For Experiments B and C the peaks appear for the load case for which the sediment pit recorded a significant amount of bed load for the first time (load case 4). Therefore, it should have been expected to see an increase

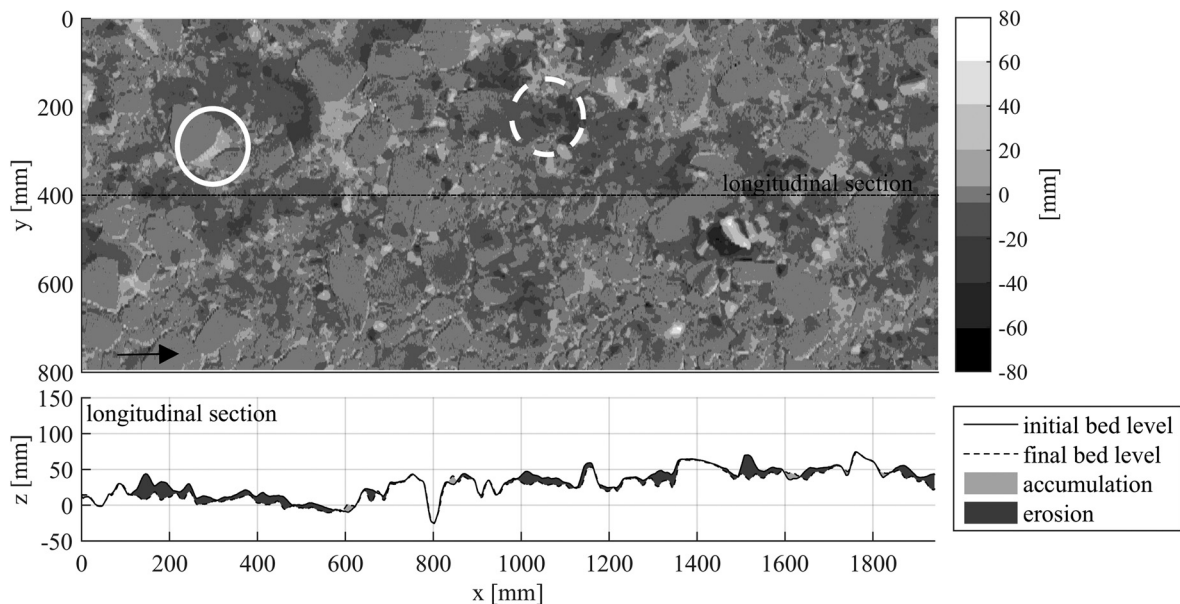


Fig. 9. Erosion (dark gray) and accumulation (light gray) areas at the end of Experiment A; full-lined circle indicates typical accumulation of finer fractions behind larger stones, and dash-lined circle indicates extensive erosion of finer fractions in unprotected areas

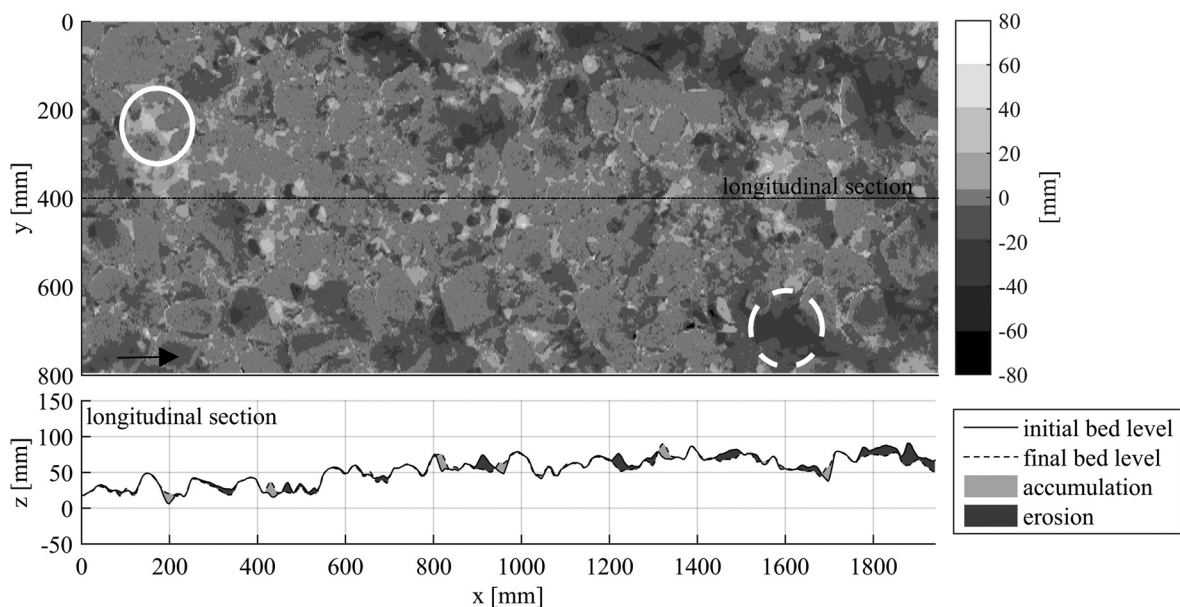


Fig. 10. Erosion (dark gray) and accumulation (light gray) areas at the end of Experiment B; full-lined circle indicates typical accumulation of finer fractions behind larger stones, and dash-lined circle indicates extensive erosion of finer fractions in unprotected areas

in the roughness and thus a lowering of the PDF curve instead of a peak. At this point, no explanation can be given for this behavior.

In all cases the probability densities are equally distributed around the zero mean value with slightly different maximum probability densities between the experiments from 0.035 to 0.040. While the standard deviation of the bed elevations σ_z remains nearly constant over the load cases of an experiment, it varies between the three experiments with a mean $\sigma_z = 20.1$ mm for Experiment A, a mean $\sigma_z = 16.53$ mm for Experiment B, and a mean $\sigma_z = 24.05$ mm for Experiment C. All PDFs show a wide range of bed elevations with a relatively high value of the probability density even for elevations ± 50 mm. Based on these

findings, the resulting PDFs confirm the high roughness of the bed surface due to the given wide-graded material as it is visually indicated by the DEMs in Fig. 4.

These results are in contrast to those of Aberle and Nikora (2006), who conducted similar experiments with successively increasing discharge in a tilting flume. They showed that the range of bed elevations and the standard deviation increase with rising discharge. Alternatively, Mao et al. (2011) performed experiments that provided varying results depending on either a static or a mobile armor layer development. With static armor layers the shape and distribution of the PDFs as well as the standard deviation remained almost constant despite increasing discharge, which is

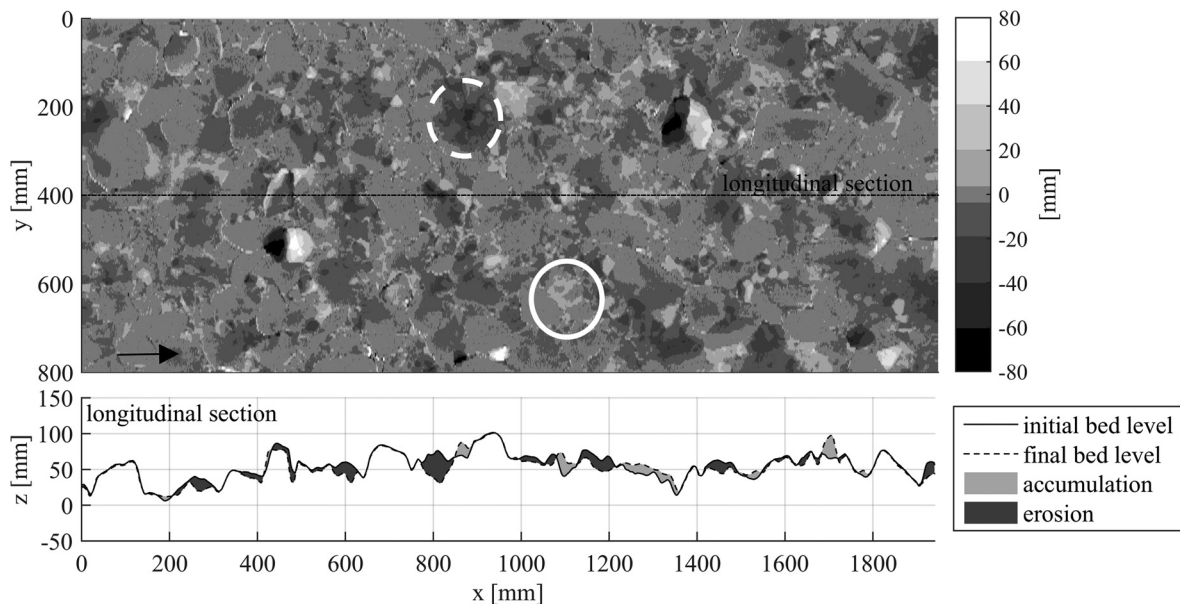


Fig. 11. Erosion (dark gray) and accumulation (light gray) areas at the end of Experiment C; full-lined circle indicates typical accumulation of finer fractions behind larger stones, and dash-lined circle indicates extensive erosion of finer fractions in unprotected areas

Table 6. Volume of Cumulated Erosion Relative to Reference Measurements at the Beginning of Each Experiment and the Averaged Erosion Height for all Load Cases and Experiments

Load case	Experiment A		Experiment B		Experiment C	
	Cumulated erosion (cm ³)	Erosion, averaged over scan area (mm)	Cumulated erosion (cm ³)	Erosion, averaged over scan area (mm)	Cumulated erosion (cm ³)	Erosion, averaged over scan area (mm)
1	—	—	288	0.19	140	0.10
2	-605	-0.39	603	0.39	421	0.27
3	-659	-0.43	439	0.28	509	0.33
4	-822	-0.53	1493	0.97	1361	0.88
5	-337	-0.22	2660	1.72	2341	1.52
6	954	0.62	4060	2.63	3519	2.28
7	2115	1.37	5596	3.63	5042	3.27

Note: Due to subsequent settlement of the bed after Load Case 1 in Experiment A, the cumulated erosion is referred to the first load case instead of reference measurements at the beginning. Negative erosion means accumulation. Values are based on DEMs. In each load case the sediment bed was exposed to the flow for approximately 2 h.

similar to the results shown in this paper. Considering the standard deviation of bed elevations as a measure of the vertical roughness length and by analysis of the statistical properties of the PDFs, Mao et al. (2011) concluded that higher discharges lead to coarser static armor layers, but at the same time the relative bed roughness remains constant.

In the present study, due to the given wide-graded material with fractions up to 200 mm, the initial bed roughness was already very high. Furthermore, only fine fractions were moved, while coarse grains, which made up a high percentage of the bed surface, remained in their original position. Except for the highest load case of Experiments B and C (Fig. 12) the influence of higher velocities on the bed roughness appears to be small. Since a significant coarsening of the surface has been visually observed, the suitability of PDFs as a practical method to analyze the development of the bed topography may be questioned to be fully representative for the given material properties and test conditions. However, the results of the highest load case suggest that an

increase in the bed roughness could be measured under even higher velocities. The evaluation of second-order structure functions (Aberle and Nikora 2006) and concurrent higher flow velocities might provide further insight into the development of the surface structure.

Fractional Critical Bed-Shear Stress

All sediment mixtures show a strong variation of the critical shear stresses $\tau_{c,i}$ with the grain size d_i . A similar dependence of the shear stress on the grain size was demonstrated by Kuhnle (1993), Wilcock (1993), and Wilcock and Crowe (2003).

Kuhnle (1993) investigated the incipient motion of sand-gravel sediment mixtures, which contained a gravel mix ($d_{50} = 5.579$ mm) and a sand mix ($d_{50} = 0.476$ mm). He found that in beds consisting of only the sand or the gravel mix, all fractions were moved by nearly the same bed-shear stress. However, in the bimodal sediment mixtures

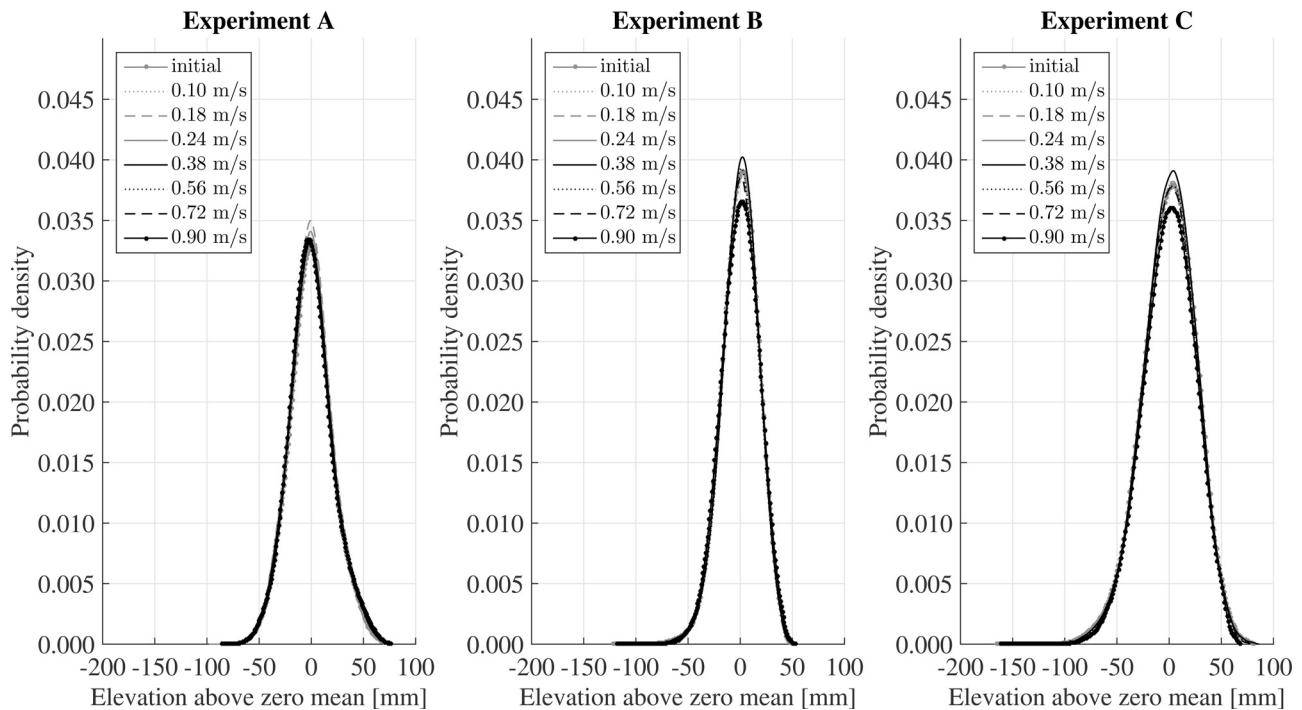


Fig. 12. Probability density functions of surface elevations at the end of each load case

Table 7. Dimensionless Critical Bed-Shear Stress $\tau_{c,i}^*$ and Corresponding Grain Size Diameter d_i for the Last Four Load Cases

Load case	Experiment A		Experiment B		Experiment C	
	d_i (mm)	$\tau_{c,i}^*$ (-)	d_i (mm)	$\tau_{c,i}^*$ (-)	d_i (mm)	$\tau_{c,i}^*$ (-)
4	0.8	0.0954	0.7	0.0720	0.6	0.0722
5	2.0	0.0909	2.2	0.0453	2.8	0.0382
6	16.0	0.0192	8.0	0.0271	6.5	0.0346
7	28.0	0.0151	17.0	0.0186	7.4	0.0596

the critical shear stress $\tau_{c,i}$ for the gravel fractions was significantly dependent on the grain size and increased with rising d_i , while the sand fractions still were moved at nearly the same bed-shear stress.

Wilcock and Crowe (2003) presented critical shear stresses for additional sand-gravel mixtures. They demonstrated that the dependency of the critical shear stress $\tau_{c,i}$ on the grain size d_i increases with the amount of sand within the mixture. Thus the extent of the shear stress variation was strongly related to the increase of nonuniformity of the sediment mixture, which can be expressed by σ_g . In line with those results, the critical shear stresses for the extremely wide-graded materials used in this paper vary strongly with grain size, indicating a highly selective mobility of individual fractions.

Kuhnle (1993) and Wilcock and Crowe (2003) illustrated the critical shear stress $\tau_{c,50}$ for the median diameter of the sediment d_{50} , which was located relatively close to the corresponding Shields value in all samples. Because only grain sizes d_i smaller than the median diameter d_{50} were collected in this present study, the critical shear stresses $\tau_{c,50}$ for the material mixtures could not be determined. It can be argued that the $\tau_{c,50}$ for the given material samples would have been much lower compared with the Shields approach. However, this conjecture is based on limited data and therefore on data extrapolation. It has to be noted that the d_{50} of all material mixtures was much larger in this study than in the experiments of Kuhnle (1993) and Wilcock and Crowe (2003).

Comparison with Existing Results and Approaches

According to Eqs. (2) and (4), existing hiding functions for the description of selective mobility of nonuniform sediments can be divided on the basis of the considered reference size fraction d_R . For the following comparison the dimensionless critical shear stresses $\tau_{c,i}^*$ for the measured grain size fractions d_i are shown in Table 7.

Approaches Based on the Reference Size d_a

Attempts by Egiazaroff (1965), Ashida and Michiue (1971), and Hayashi et al. (1980) are based on the arithmetic mean grain size d_a [Eq. (11)] with the dimensionless critical shear stress $\tau_{c,a}^*$, which reads

$$\tau_{c,a}^* = \frac{\tau_{c,a}}{(\rho_s - \rho)gd_a} \quad (7)$$

with $\tau_{c,a}$ as the critical shear stress of the arithmetic mean grain size d_a .

The approach can be rewritten (Egiazaroff 1965) as

$$\frac{\tau_{c,i}^*}{\tau_{c,a}^*} = \left[\frac{\log 19}{\log(19d_i/d_a)} \right]^2 \quad (8)$$

Ashida and Michiue (1971) modified the approach by Egiazaroff (1965) for relations $d_i/d_a < 0.40$. It can be expressed as

$$\frac{\tau_{c,i}^*}{\tau_{c,a}^*} = 0.85 \left(\frac{d_i}{d_a} \right)^{-1} \quad (9)$$

Hayashi et al. (1980) suggested the following critical condition for a nonuniform sediment mixture:

$$\frac{\tau_{c,i}^*}{\tau_{c,a}^*} = \begin{cases} \left[\frac{\log 8}{\log(8 d_i/d_a)} \right]^2, & \text{for } d_i/d_a \geq 1.0 \\ \frac{1}{d_i/d_a}, & \text{for } d_i/d_a \leq 1.0 \end{cases} \quad (10)$$

On the basis of measurement data, Misri et al. (1984) calculated values of $\tau_{c,a}^* = 0.023\text{--}0.0303$ for the use of the approaches by Egiazaroff (1965) and Hayashi et al. (1980), instead of $\tau_{c,a}^* = 0.06$, which was used by Egiazaroff (1965) and is apparently too large (Wu et al. 2000). Furthermore Garde and Ranga Raju (1985) proposed an averaged value of $\tau_{c,a}^* = 0.03$. To calculate the fractional critical shear stress $\tau_{c,i}^*$ and for the purpose of comparison, a constant value of $\tau_{c,a}^* = 0.03$ is used in this study for the approaches of Egiazaroff (1965), Ashida and Michiue (1971), and Hayashi et al. (1980).

In this study the arithmetic mean size d_a is calculated by $d_i = \sqrt{d_1 d_2}$, which is the geometric mean size of the boundaries d_1 and d_2 of the considered grain fraction

$$d_a = \frac{1}{100} \sum \Delta p_i d_i \quad (11)$$

As shown in Fig. 13, all approaches clearly over predict the dimensionless critical shear stress $\tau_{c,i}^*$ for all relations d_i/d_a . For the material mixtures given in this study $\tau_{c,a}^*$ values between 0.011 and 0.0284 can be found, which are considerably smaller than the proposed value of $\tau_{c,a}^* = 0.03$.

Approaches Based on the Reference Size d_{50}

The median diameter d_{50} as reference size for the determination of $\tau_{c,i}^*$ was used in many approaches present in literature. Usually those approaches can be expressed in the form

$$\tau_{c,i}^* = \alpha \left(\frac{d_i}{d_{50}} \right)^{-\beta} \quad (12)$$

with the coefficient α representing the value of the dimensionless critical shear stress $\tau_{c,50}^*$ (reference Shields stress) of the d_{50} diameter and β as the exponent.

Table 8 summarizes the approaches used as comparison. In addition to the median diameter d_{50} the coefficient α and the exponent

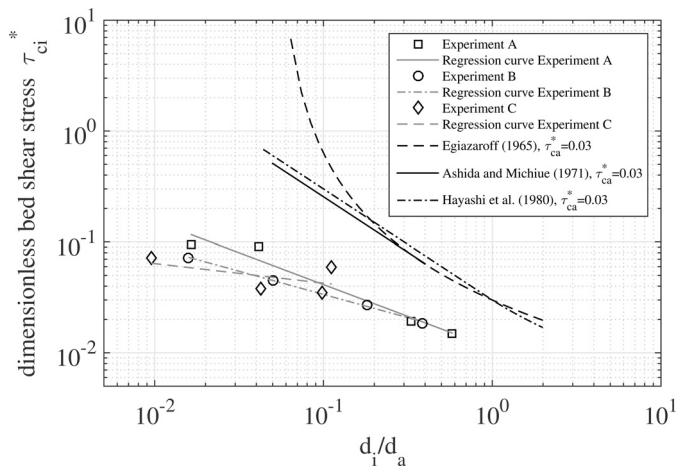


Fig. 13. Comparison of measured dimensionless critical shear stresses $\tau_{c,i}^*$ with approaches of Egiazaroff (1965), Ashida and Michiue (1971), and Hayashi et al. (1980) with d_a as reference size

β are given in Table 8. While Andrews (1983) obtained $\tau_{c,i}^*$ by applying LGM, which was also used in this study, Parker et al. (1982b) and Kuhnle (1993) defined $\tau_{c,i}^*$ by using a RTM. As Wilcock (1988) pointed out, a comparison of both methods could be subject to uncertainties, which may be associated to inevitable scaling problems in estimating the initial motion condition for individual fractions in nonuniform sediments.

As remarked earlier, all approaches significantly over predict the dimensionless critical shear stress $\tau_{c,i}^*$ for all d_i/d_{50} values for the considered sediment mixture (see Fig. 14). The values of coefficient α are much smaller (0.0145–0.0279) than the values suggested by the given approaches (see Table 8) and compared with the reference Shields stress of $\tau_{c,50}^* = 0.055$.

Furthermore the slopes (exponent β) of the fitting curves for the results of the present experiments are less steep compared with the existing approaches and significantly deviate from unity. An even higher selective mobility for the used wide-graded material mixtures is indicated, as would have been estimated by the existing approaches.

Comparison with approaches considering d_a and d_{50} as reference size proves that the use of a reference size only based on a single representative grain size does not represent the characteristics and erosion stability of extremely wide-graded material mixtures adequately. The stability behavior of the tested material compositions under flow condition, which has been observed during the

Table 8. Comparison of Coefficient α and Exponent β of Least-Square Fitting to $\tau_{c,i}^* = \alpha (d_i/d_{50})^{-\beta}$

Data series	d_{50} (mm)	Coefficient α (-)	Exponent β (-)
Experiment A	30	0.0145	0.573
Experiment B	25	0.0163	0.419
Experiment C	72	0.0279	0.176
Andrews (1983)	25–74	0.0834	0.872
Parker et al. (1982b)	20	0.0876	0.982
Kuhnle (1993) SG45 sand	0.4	0.0447	1.041
Kuhnle (1993) SG45 gravel	5.6	0.0369	0.420

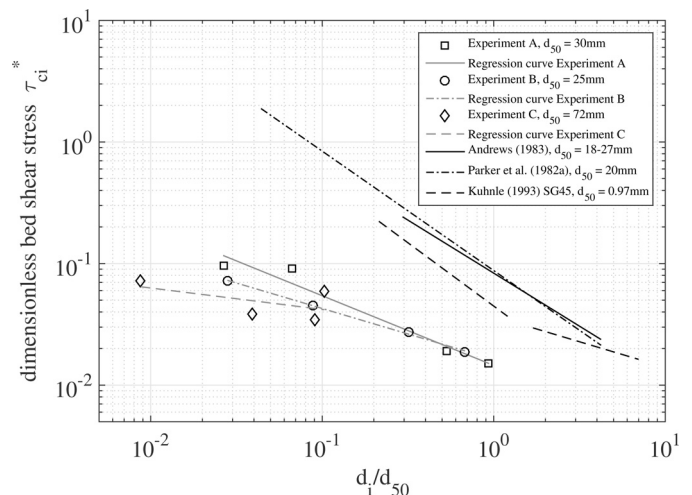


Fig. 14. Comparison of experimental data with results of Andrews (1983), Parker et al. (1982b), and Kuhnle (1993) with d_{50} as reference size

experiments, is not satisfactorily represented by existing approaches, which lack universality with respect to d_a and d_{50} .

Approaches Based on the Reference Size d_σ

Recently, Patel et al. (2013) reviewed the applicability of several approaches given in the literature (i.e., Parker et al. 1982b; Wilcock 1993; Wu et al. 2000) and determined those to be less accurate for bimodal and nonuniform material mixtures. To account for bimodal material properties they proposed a relationship for the dimensionless critical shear stress $\tau_{c,i}^*$ based on the geometric standard deviation σ_g as reference size

$$\tau_{c,i}^* = \alpha \left(\frac{d_i}{d_\sigma} \right)^{-\beta} \quad (13)$$

$$d_\sigma = d_g \sigma_g \quad (14)$$

with d_σ as the product of the geometric mean size d_g and the geometric standard deviation σ_g . In reference to Patel et al. (2013, 2014) the

Table 9. Comparison of Coefficient α and Exponent β of Least-Square Fitting to $\tau_{c,i}^* = \alpha (d_i/d_g)^{-\beta}$

Data series	d_g (mm)	σ_g (-)	Coefficient α (-)	Exponent β (-)	R^2 (-)
Experiment A	22.46	5.79	0.0063	0.573	0.88
Experiment B	17.65	6.74	0.0085	0.419	0.99
Experiment C	35.96	5.95	0.0231	0.176	0.55
Wilcock et al. (2001) BOMC	3.25	5.90	0.011	0.37	0.96
Wilcock et al. (2001) J27	6.06	3.91	0.012	0.53	0.91
Patel et al. (2014) SD4.5	3.02	4.46	0.009	0.52	0.99

Note: Parameter for Wilcock et al. (2001) obtained from Patel et al. (2013). BOMC = bed of many colors.

parameters d_g and σ_g in this study have been calculated by using the ψ scale. For further details the authors refer to Patel et al. (2013).

For the purpose of comparison available sediment mixtures were chosen, which are characterized by high σ_g values similar to those in the present study (Table 9). The coefficients α and β for these mixtures were obtained from Patel et al. (2013), who provided these parameters for unimodal and bimodal sediments used in several available experiments.

By considering the geometric standard deviation σ_g within the reference size, a good agreement with similar wide-graded material mixtures has been achieved as shown in Table 9 and demonstrated by Fig. 15. For materials with significantly smaller σ_g (Kuhnle 1993, SG45) much higher values of β are obtained.

In view of the previous comparisons, the dependence of the reproducibility and the comparability of wide-graded material properties on the selected reference size become apparent. The properties of the material mixtures in this study were significantly better represented by using d_σ as reference size. The depicted experiments and findings thereof in the present paper are in line with work conducted by Patel et al. (2013, 2014), and thus prove independently the approach of using d_σ as reference size to account for graded-material properties. In addition, Patel and Ranga Raju (1999) showed a strong decrease of $\tau_{c,i}^*$ with increasing σ_g . They explained the dependence by the fact that an increase of σ_g leads to a larger range of grain sizes. Thus the mean grain size d_σ might be subject to an increasing exposure and tends to erode by a smaller critical shear stress.

In contrast to the results of Patel et al. (2013), Chin et al. (1994) found that a simple description of the armor layer based on the geometric standard deviation could be inadequate. They showed that the formation of the armor layer is strongly dependent on the coarser 16% of the grain size distribution. Thus a reference size that considers only grain sizes smaller than the d_{84} grain size would not be sufficient. They suggested relating the dimensional critical shear to the ratio of the maximum grain size and the median grain size of the parent material. Therefore, future studies will be performed to evaluate further reference sizes and to define parameters, which can describe the material behavior adequately.

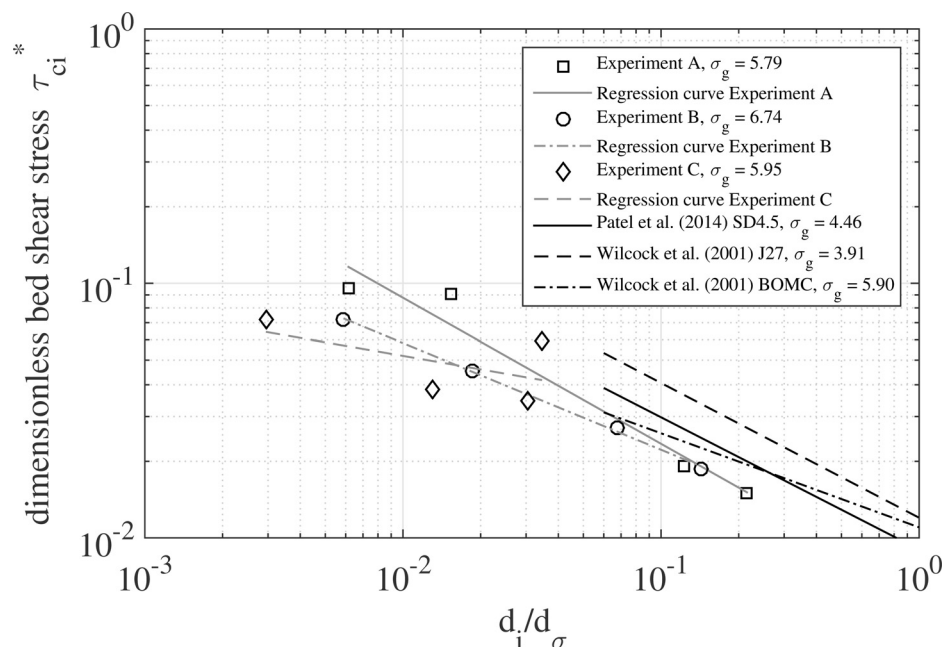


Fig. 15. Comparison of experimental data with results of Wilcock et al. (2001) and Patel et al. (2014) with d_σ as reference size

Discussion

Instead of completing a whole new bed for each load case, the tests were performed by successively increasing the flow velocity. This preload might have some implications on the sediment mobility and stability, which could reduce the comparability of the results with other studies. The amount of transported bed load could be reduced and the grain size distribution altered in comparison to a setup with new sediment beds, because a large portion of finer fractions was eroded during the previous load case. The determination of meaningful sediment transport rates is made more difficult, particularly as the temporal evolution of erosion is affected as well. With the development of an armor layer the overall stability of the sediment bed is increased for the following load, affecting the critical shear stress for some particles. At the same time, the successive load enabled the investigation of successive development of stable armor layers and their destruction. Eventually, as a consequence of the material characteristics, it was not possible to reproduce a consistent and comparable sediment bed for each load case (cf. Fig. 4). The combination of inhomogeneous material properties and uneven installation of new sediment beds for each load case would have complicated the analysis.

The coarsening of the bed surface and the development of an armor layer during the experiments could be verified by visual observation. Furthermore, as a former component, the eroded bed material reflects the composition of the bed surface. Thus the coarsening of the trapped material (Fig. 8) with increasing shear stress indicates a continuous coarsening of the bed surface, which in turn can influence the flow field and the bed-shear stress. But due to occurring hiding processes, small grain fractions were still available on the bed surface, which is also visible in Fig. 8. With consistent flow intensity a stable armor layer developed over time, and with further increase of the flow velocity the armor layer was destroyed, larger stones were eroded, and the amount of small grain fractions on the bed surface was reduced. However, smaller fractions can also find new hiding options in holes left by eroded larger stones, especially in upstream sediment supply, i.e., mobile armor layer. The recurring process of erosion and armoring took place only in the top layer of the bed surface, which was directly exposed to the flow. Under this top layer the grain size distribution of the initial bed remained preserved, which could be observed during the replacement of the material bed.

The coarsening of the bed could not be reproduced in the development of PDFs of the bed elevations as presented by Aberle and Nikora (2006) and Mao et al. (2011). In contrast to those investigations, the extremely wide-graded quarry-stone material used in the present study presumably led to a fairly stable bed surface that contained a high proportion of large and nonmoving fractions. The sole quantification of the bed surface characteristics by PDFs is not sufficient for these conditions. Therefore, to allow a comprehensive assessment of the changes of the bed surface an additional determination of the composition of the surface grain size distribution is needed and will be applied in future studies. Moreover, in view of a better understanding of the processes involved in the formation of the erosion stability, fundamental studies on the surface grain size distribution for this kind of material as well as more detailed velocity and turbulence measurements are necessary.

With respect to the Shields approach, the critical shear stresses for the considered fractions, which are all well below the d_{50} median diameter, seem relatively small. The shear stresses $\tau_{c,50}$ for the median diameter based on the reference Shields stress of $\tau_{c,50}^* = 0.055$ would have been between 22.26 (Experiment B) and 64.09 N/m² (Experiment C). As already pointed out by several authors and

shown in summary by Shvidchenko et al. (2001), the Shields curve is not an appropriate way to accurately assess the incipient motion of nonuniform sediment mixtures. However, the dimension of the differences by which the behavior of the tested sediment mixture deviates from the prediction of the Shields curve remains rather unexpected. Given the explained method, uncertainties in the estimation of the bed-shear stresses would be conceivable, especially concerning the extremely rough surface structure. However, the application of the log law fitting has shown reasonable results, with high coefficients of determination. The same applies to the roughness lengths, which were determined during the shear stress estimation for each ADV measurement position. The results were in good agreement with the actual roughness of the bed and the grain size distribution of the material mixtures, but regarding the rough surface and the consequential fluctuating shear stress distribution, a focus on a detailed and global resolution of the flow conditions closer to bed might have been a useful addition for the bed-shear stress determination.

The comparison with available approaches for the incipient motion of nonuniform materials revealed considerable differences in the ability to reproduce the characteristics of extremely wide-graded material mixtures. While approaches based on either the arithmetic mean diameter d_a or the median size d_{50} do not seem to represent the material characteristics adequately, and because they tend to over predict $\tau_{c,i}^*$, the use of d_σ as reference size, as introduced by Patel and Ranga Raju (1999), performs much better in terms of accordance with results from other studies. Overall, it should be noted that the comparability with other studies is quite limited. First, different methods for the determination of the critical bed-shear stresses (LGM and RTM) have been used throughout the available studies, which could induce uncertainties due to scaling problems, as pointed out by Wilcock (1988). More importantly, the material and test conditions of this study significantly differ from all existing studies. Materials with round edges and fairly even grain size distribution, which can be found in natural rivers, were used. The material used in this study was fabricated of quarry-stone material with sharp edges and an exceptionally wide-graded grain size distribution, which may be applied mostly in coastal and offshore areas as scour and bed protection systems. While the influence of the nonuniformity of the material mixture on the incipient motion (Wilcock and Crowe 2003) and on the scour development (Ettema 1976; Chiew 1984; Baker 1986) was proven, the influence of the particle shape is mostly unknown. Göğüş and Define (2005) performed investigations on the effect of shape on the incipient motion of solitary particles. They described the differences between shapes with a shape factor that relates the particles dimensions to each other. They found out that the shape has a significant influence on the incipient motion. However, the effect of the particle shape on incipient motion within a wide-graded sediment bed and on the ability to develop an armor layer is still unknown.

For a comparison with other studies it also has to be considered that the experiments in this study were performed without upstream sediment feeding (although some suspended sediment was recirculated). With a lack of sediment supply the flow selectively entrains finer grain sizes, leading to the development of a static armor layer (Mao et al. 2011). A highly selective mobility was also found in this study (cf. Figs. 8 and 13). Experiments with additional sediment supply, whether through recirculation or upstream sediment feeding, allow the sediment bed to form a mobile armor layer. Here, the “vertical winnowing” process, in which finer fractions tend to fall in voids created by the entrainment of larger fractions, is leading to an over exposition of larger fractions. As a result, a mobile armor layer equalizes the mobility between small and large fractions (Parker

et al. 1982a). This could influence the results of this study in such a way that the critical shear stresses might show a significant lower dependency on the grain size, in other words equal mobility. As anticipated only the fine fractions have been eroded, while the largest grain fractions have not been entrained at all. Furthermore, the finer fractions partially possess a cohesive character. Once suspended a sedimentation of those grain fractions is unlikely due to their small grain sizes and the high velocities. Therefore, a consistent sediment feeding with this kind of material was difficult to implement under given conditions. But since the investigation of a more mobile bed is of great interest, future studies in a tilting flume are planned, which will give the option of higher velocities and additional sediment feeding.

Conclusions

Hydraulic model tests were conducted to research the influence of wide-graded material effects on the erosion stability of bed and scour protection. The wide-graded quarry-stone material was examined under unidirectional current and the critical shear stresses were determined with the intention to facilitate future scour protection design.

To assess the stability of this material, the process of erosion due to successively increasing flow velocity has been described. Using DEMs (Figs. 9–11) it could be shown that the amount and distribution of erosion correlates well with the surface of the bed, i.e., with the concentration of finer fractions on the bed surface.

Furthermore, the grain size distributions of the eroded sediment (Fig. 8) indicate a continuously coarsening of the eroded bed load. However, on average, only a cumulated erosion between 1.4 mm for Experiment A and 3.6 mm for Experiment B could be measured. However, because of its heterogeneous appearance, this erosion should not be mistaken as a general lowering of the bed, which could not be determined despite starving bed setup without additional sediment supply.

At incipient motion the material showed a strong variation of fractional critical shear stress $\tau_{c,i}$ with grain size d_i , which points to a highly selective mobility of individual fractions and, therefore, is an indication to the development of a static armor layer. The shear stress was estimated from local velocity measurements by applying the log law method. Despite the nonuniformity of the flow, a reasonable compliance of the measured velocities with the log law was found (Fig. 6). The comparison of the critical shear stresses with existing approaches for nonuniform sediments revealed the importance of the selection of an appropriate reference size fraction to account for the characteristics of extremely wide-graded material mixtures. While usage of d_{50} and d_a as reference size fails to represent the material characteristics adequately, the use of d_σ as reference size performs well if compared with results from previous studies.

In summary, the selective erosion of finer grain sizes could be determined, which in turn led to a coarsening of the bed and the development of a stabilizing armor layer. The remaining larger grain sizes provided the required stability of the bed against the applied hydraulic loading. Therefore, this study demonstrates the potential of wide-graded material for a dynamic design of scour protection, which allows the limited movement of stones to reduce the required stone size and decrease the cost. Following the erosion of finer fractions and the formation of an armor layer, the remaining coarse bed could assure the stabilizing function of the cover layer.

Since the erosion mechanisms in such complex sediment mixtures, which lead to the demonstrated stability, are still not fully understood, future studies will focus on the stabilizing processes by

performing detailed measurements of the flow above such rough beds and by determining the grain size distribution and bed surface structure at several stages during the armor layer development. Furthermore, the definition of more suitable reference sizes for the determination of incipient motion of wide-graded quarry-stone material will be an integral part of future studies.

Acknowledgments

The authors are thankful to Mibau Holding GmbH for supporting this research and Dr. K. Peters for stimulating remarks during the research. Furthermore, the authors thank T. Freitag and M. Bartels for their support in conducting the extensive hydraulic experiments.

Notation

The following symbols are used in this paper:

- C_c = dimensionless curvature coefficient;
- C_u = dimensionless coefficient of uniformity;
- C_1 = dimensionless proportionality constant ($C_1 = 0.19$);
- d = vertical displacement height;
- d_a = arithmetic mean grain diameter of sediment mixture;
- d_g = geometric mean diameter of sediment mixture;
- d_i = grain diameter of considered fraction in a sediment mixture;
- d_R = considered reference grain diameter;
- d_σ = representative diameter;
- d_{16} = grain size for which 16% of the material by weight is finer;
- d_{50} = grain size for which 50% of the material by weight is finer;
- d_{84} = grain size for which 84% of the material by weight is finer;
- d_{90} = grain size for which 90% of the material by weight is finer;
- f_i = proportion of fraction i in the bed material;
- g = acceleration due to gravity;
- H = water depth;
- I = slope of channel;
- k = turbulent kinetic energy;
- k_s = equivalent sand roughness;
- p_i = percentage by weight corresponding to d_i ;
- q_{si} = is the sediment transport rate for the fraction i ;
- R = hydraulic radius;
- R^2 = coefficient of determination;
- T = duration of load case;
- u = velocity at height z above the bed;
- u_1, u_2 = velocities at height z_1 and z_2 above the bed;
- u' = turbulent component of streamwise velocity u ;
- u_* = shear velocity;
- \bar{u} = cross-sectional averaged mean flow velocity;
- $\overline{u'w'}$ = Reynolds stress;
- v' = turbulent component of lateral velocity w ;
- W_i^* = dimensionless bed load parameter for a particular size fraction i ;
- w' = turbulent component of vertical velocity w ;
- x, y = coordinates in flow and in transverse direction;
- z = height above the bed;
- z_0 = roughness length;
- z_1, z_2 = bed-nearest position of velocity measurement;
- α = dimensionless coefficient in hiding functions;

- β = dimensionless exponent in hiding functions;
 κ = Karman-Constant;
 ρ = density of water;
 ρ_s = density of sediment;
 σ_g = geometric standard deviation of the sediment mixture;
 σ_z = geometric standard deviation of the bed elevations;
 $\tau_{c,d}^*$ = dimensionless critical bed-shear stress for the arithmetic mean diameter d_a ;
 $\tau_{c,i}$ = critical bed-shear stress for the fraction i ;
 $\tau_{c,i}^*$ = dimensionless critical bed-shear stress for the fraction i ;
 $\tau_{c,R}^*$ = dimensionless critical bed shear for the reference size d_R ;
 $\tau_{c,50}$ = critical bed shear for the median grain diameter d_{50} ;
 $\tau_{c,50}^*$ = dimensionless critical bed shear for the median grain diameter d_{50} ;
 τ_0 = bed-shear stress; and
 $\bar{\tau}_0, \tau_{std}$ = mean and standard deviation value of estimated bed-shear stresses.

References

- Aberle, J., and Nikora, V. (2006). "Statistical properties of armored gravel bed surfaces." *Water Resour. Res.*, 42(11), 414. [10.1029/2005WR004674](#)
- Andrews, E. D. (1983). "Entrainment of gravel from naturally sorted riverbed material." *Geol. Soc. Am. Bull.*, 94(10), 1225–1231. [10.1130/0016-7606\(1983\)94<1225:EOGFS>2.0.CO;2](#)
- Ashida, K., and Michiue, M. (1971). "An investigation of the river bed degradation of a dam." *Proc., 14th Congress of the IAHR*, Paris, France, 3, 247–255.
- Bagherimiyab, F., and Lemmin, U. (2013). "Shear velocity estimates in rough-bed open-channel flow." *Earth Surf. Process. Landforms*, 38(14), 1714–1724. [10.1002/esp.3421](#)
- Baker, R. (1986). "Local scour at bridge piers in non-uniform sediment." Master thesis, School of Engineering, Univ. of Auckland, Auckland, New Zealand.
- Biron, P. M., Robson, C., Lapointe, M. F., and Gaskin, S. J., (2004). "Comparing different methods of bed shear stress estimates in simple and complex flow fields." *Earth Surf. Process. Landforms*, 29(11), 1403–1415. [10.1002/esp.1111](#)
- Cao, Z., Pender, G., and Meng, J. (2006). "Explicit formulation of the Shields diagram for incipient motion of sediment." *J. Hydraul. Eng.*, 132(10), 1097–1099. [10.1061/\(ASCE\)0733-9429\(2006\)132:10\(1097\)](#)
- Carling, P. A. (1983). "Threshold of coarse sediment transport in broad and narrow natural streams." *Earth Surf. Process. Landforms*, 8(1), 1–18. [10.1002/esp.3290080102](#)
- Chiew, Y. M. (1984). "Local scour at bridge piers." Doctoral thesis, School of Engineering, Univ. of Auckland, Auckland, New Zealand.
- Chin, C. O., Melville, B. W., and Raudkivi, A. J. (1994). "Streambed armor-ing." *J. Hydraul. Eng.*, 120(8), 899–918. [10.1061/\(ASCE\)0733-9429\(1994\)120:8\(899\)](#)
- Coleman, S. E., and Nikora, V. I. (2008). "A unifying framework for particle entrainment." *Water Resour. Res.*, 44(4). [10.1029/2007WR006363](#)
- De Schoesitter, P., Audenaert, S., Baelus, L., Bolle, A., Brown, A., Das Neves, L., et al. (2014). "Feasibility of a dynamically stable rock armour layer scour protection for offshore wind farms." *Proc., 33rd Int. Conf. on Offshore Mechanics and Arctic Engineering—OMAE, ASME*, Vol. 3, Offshore Geotechnics, San Francisco.
- De Vos, L. (2008). "Optimisation of scour protection design for monopoles and quantification of wave run-up—engineering the influence of an offshore wind turbine on local flow conditions." Doctoral thesis, Faculty of Engineering, Ghent University, Belgium.
- De Vos, L., De Rouck, J., Troch, P., and Frigaard, P. (2011). "Empirical design of scour protection around monopile foundations: Part 1: Static approach." *Coastal Eng.*, 58(6), 540–553. [10.1016/j.coastaleng.2011.02.001](#)
- De Vos, L., De Rouck, J., Troch, P., and Frigaard, P. (2012). "Empirical design of scour protection around monopile foundations: Part 2: Dynamic approach." *Coastal Eng.*, 60(1), 286–298. [10.1016/j.coastaleng.2011.11.001](#)
- Egiazaroff, I. V. (1965). "Calculation of nonuniform sediment concentration." *J. Hydraul. Div.*, 91(4), 225–247.
- Ettema, R. (1976). "Influence of bed material gradation on local scour." M.S. thesis, School of Engineering, Univ. of Auckland, Auckland, New Zealand.
- Garde, R. J., and Ranga Raju, K. G. (1985). *Mechanics of sediment transportation and alluvial stream problems*, 2nd Ed., Wiley Eastern Limited, New Delhi, India.
- Gögüş, M., and Define, Z. (2005). "Effect of shape on incipient motion of large solitary particles." *J. Hydraul. Eng.*, 131(1), 38–45.
- Goseberg, N., Wurpts, A., and Schlurmann, T. (2013). "Laboratory-scale generation of tsunami and long waves." *Coastal Eng.*, 79, 57–74. [10.1016/j.coastaleng.2013.04.006](#)
- Hayashi, T. S., Ozaki, S., and Ichibashi, T. (1980). "Study on bed load transport of sediment mixture." *Proc., 24th Japanese Conf. on Hydraulics* (in Japanese), Japan Society of Civil Engineers.
- Jain, S. C. (1990). "Armor or pavement." *J. Hydraul. Eng.*, 116(3), 436–440. [10.1061/\(ASCE\)0733-9429\(1990\)116:3\(436\)](#)
- Kim, S. C., Friedrichs, C. T., Maa, J. P. Y., and Wright, L. D. (2000). "Estimating bottom stress in tidal boundary layer from acoustic Doppler velocimeter data." *J. Hydraul. Eng.*, 126(6), 399–406. [10.1061/\(ASCE\)0733-9429\(2000\)126:6\(399\)](#)
- Komar, P. D. (1987). "Selective grain entrainment by a current from a bed of mixed sizes: A reanalysis." *J. Sediment. Petrol.*, 57(2), 203–211.
- Kothyari, U. C., and Jain, R. K. (2008). "Influence of cohesion on the incipient motion condition of sediment mixtures." *Water Resour. Res.*, 44(4). [10.1029/2007WR006326](#)
- Kuhnle, R. A. (1993). "Incipient motion of sand-gravel sediment mixtures." *J. Hydraul. Eng.*, 119(12), 1400–1415. [10.1061/\(ASCE\)0733-9429\(1993\)119:12\(1400\)](#)
- Mao, L., Cooper, J. R., and Frostick, L. E. (2011). "Grain size and topographical differences between static and mobile armour layers." *Earth Surf. Process. Landforms*, 36(10), 1321–1334. [10.1002/esp.2156](#)
- Marion, A., and Fraccarollo, L. (1997). "Experimental investigation of mobile armor development." *Water Resour. Res.*, 33(6), 1447–1453. [10.1029/97WR00705](#)
- Marion, A., Tait, S. J., and McEwan, I. K. (2003). "Analysis of small-scale gravel bed topography during armoring." *Water Resour. Res.*, 39(12). [10.1029/2003WR002367](#)
- Melville, B. W., and Sutherland, A. J. (1988). "Design method for local scour at bridge piers." *J. Hydraul. Eng.*, 114(10), 1210–1226. [10.1061/\(ASCE\)0733-9429\(1988\)114:10\(1210\)](#)
- Misri, R. L., Garde, R. J., and Ranga Raju, K. G. (1983). "Experiments on bed load transport of nonuniform sands and gravels." *Proc., 2nd Int. Symp. on River Sedimentation*, Nanjing, China.
- Misri, R. L., Ranga Raju, K. G., and Garde, R. J. (1984). "Bed load transport of coarse nonuniform sediment." *J. Hydraul. Eng.*, 110(3), 312–328. [10.1061/\(ASCE\)0733-9429\(1984\)110:3\(312\)](#)
- Nielsen, A. W., Liu, X., Sumer, B. M., and Fredsøe, J. (2013). "Flow and bed shear stresses in scour protections around a pile in a current." *Coastal Eng.*, 72, 20–38. [10.1016/j.coastaleng.2012.09.001](#)
- Nikora, V., and Goring, D. (2000). "Flow turbulence over fixed and weakly mobile gravel beds." *J. Hydraul. Eng.*, 126(9), 679–690. [10.1061/\(ASCE\)0733-9429\(2000\)126:9\(679\)](#)
- Parker, G., Dhamotharan, S., and Stefan, H. (1982a). "Model experiments on mobile, paved gravel bed streams." *Water Resour. Res.*, 18(5), 1395–1408.
- Parker, G., Klingeman, P. C., and McLean, D. G. (1982b). "Bedload and size distribution in paved gravel-bed streams." *J. Hydraul. Div.*, 108(4), 544–571.
- Parker, G., and Sutherland, A. J. (1990). "Fluvial armor." *J. Hydraul. Res.*, 28(5), 529–544. [10.1080/00221689009499044](#)

- Patel, P., and Ranga Raju, K. G. (1999). "Critical tractive stress of nonuniform sediments." *J. Hydraul. Res.*, 37(1), 39–58. [10.1080/00221689909498531](#)
- Patel, S. B., Patel, P. L., and Porey, P. D. (2013). "Threshold for initiation of motion of unimodal and bimodal sediments." *Int. J. Sediment Res.*, 28(1), 24–33. [10.1016/S1001-6279\(13\)60015-3](#)
- Patel, S. B., Patel, P. L., and Porey, P. D. (2014). "Estimation of fractional critical tractive stress from fractional bed load transport measurements of unimodal and bimodal sediments." *Measurement*, 47, 393–400. [10.1016/j.measurement.2013.08.025](#)
- Petrie, J., Diplas, P., Nam, S., and Gutierrez, M. S. (2010). "Local boundary shear stress estimates from velocity profiles measured with an ADCP." *Proc., River Flow 2010*, Ditttrich, A., Koll, K., Aberle, J., and Geisenhainer, P., eds., BAW Federal Waterways Engineering and Research Institute, Germany, 1749–1755.
- Ribberink, J. S. (1998). "Bed-load transport for steady flows and unsteady oscillatory flows." *Coastal Eng.*, 34(1–2), 59–82. [10.1016/S0378-3839\(98\)00013-1](#)
- Rowinski, P. M., Aberle, J., and Mazurczyk, A. (2005). "Shear velocity estimation in hydraulic research." *Acta Geophys. Polonica*, 53(4), 567–583.
- Schendel, A., Goseberg, N., and Schlurmann, T. (2014). "Experimental study on the performance of coarse grain materials as scour protection." *Coastal Eng. Proc.*, 1(34). [10.9753/icce.v34.structures.58](#)
- Schürenkamp, D., Oumeraci, H., Kayser, J., and Karl, F. (2014). "Numerical and laboratory experiments on stability of granular filters in marine environment." *Coastal Eng. Proc.*, 1(34). [10.9753/icce.v34.structures.17](#)
- Shields, A. (1936). "Anwendung der Ähnlichkeitsmechanik und der Turbulenzforschung auf die Geschiebepbewegung." *Mitteilungen der Preußischen Versuchsanstalt für Wasserbau und Schiffbau*, Berlin (in German).
- Shvidchenko, A. B., Pender, G., and Hoey, T. B. (2001). "Critical shear stress for incipient motion of sand/gravel streambeds." *Water Resour. Res.*, 37(8), 2273–2283. [10.1029/2000WR000036](#)
- Sumer, B. M. (2014). "A review of recent advances in numerical modelling of local scour problems." *Proc., 7th Int. Conf. on Scour and Erosion*, CRC Press, Boca Raton, FL, 61–70.
- Sumer, B. M., and Fredsøe, J. (2002). *The mechanics of scour in the marine environment*, World Scientific, Singapore.
- Sumer, B. M., and Nielsen, A. W. (2013). "Sinking failure of scour protection at wind turbine foundation." *Proc. Inst. Civ. Eng.*, 166(4), 170–188. [10.1680/ener.12.00006](#)
- Sumer, B. M., Whitehouse, R. J. S., and Tørum, A. (2001). "Scour around coastal structures: A summary of recent research." *Coastal Eng.*, 44(2), 153–190. [10.1016/S0378-3839\(01\)00024-2](#)
- van Rijn, L. C. (1993). *Principles of Sediment transport in rivers, estuaries and coast seas*, Aqua Publications, the Netherlands.
- van Rijn, L. C. (2007). "Unified view of sediment Transport by currents and waves. III: Graded beds." *J. Hydraul. Eng.*, 133(7), 761–775. [10.1061/\(ASCE\)0733-9429\(2007\)133:7\(761\)](#)
- Whitehouse, R. J. S., Harris, J. M., Sutherland, J., and Rees, J. (2011). "The nature of scour development and scour protection at offshore windfarm foundations." *Mar. Pollut. Bull.*, 62(1), 73–88. .
- Wilcock, P. R. (1988). "Methods for estimating the critical shear stress of individual fractions in mixed-size sediment." *Water Resour. Res.*, 24(7), 1127–1135. [10.1029/WR024i007p01127](#)
- Wilcock, P. R. (1993). "Critical shear stress of natural sediments." *J. Hydraul. Eng.*, 119(4), 491–505. [10.1061/\(ASCE\)0733-9429\(1993\)119:4\(491\)](#)
- Wilcock, P. R. (1996). "Estimating local bed shear stress from velocity observations." *Water Resour. Res.*, 32(11), 3361–3366. [10.1029/96WR02277](#)
- Wilcock, P. R., and Crowe, J. C. (2003). "Surface-based transport model for mixed-size sediment." *J. Hydraul. Eng.*, 129(2), 120–128. [10.1061/\(ASCE\)0733-9429\(2003\)129:2\(120\)](#)
- Wilcock, P. R., Kenworthy, S. T., and Crowe, J. C. (2001). "Experimental study of the transport of mixed sand and gravel." *Water Resour. Res.*, 37(12), 3349–3358. [10.1029/2001WR000683](#)
- Wolters, G., and van Gent, M. R. A. (2012). "Granular open filters on a horizontal bed under wave and current loading." *Proc. Coastal Eng.*, 1(33). [10.9753/icce.v33.structures.32](#)
- Wu, W., and Lin, Q. (2014). "Nonuniform sediment transport under non-breaking waves and currents." *Coastal Eng.*, 90, 1–11. [10.1016/j.coastaleng.2014.04.006](#)
- Wu, W., Wang, S. S. Y., and Jia, Y. (2000). "Nonuniform sediment transport in alluvial rivers." *J. Hydraul. Res.*, 38(6), 427–434. [10.1080/00221680009498296](#)